Building Load Control using Distributionally Robust Chance-Constrained Programs with Right-Hand Side Uncertainty and the Risk-Adjustable Variants

Yiling Zhang

Department of Industrial and Systems Engineering, University of Minnesota yiling@umn.edu

Jin Dong

Electrification and Energy Infrastructures Division, Oak Ridge National Laboratory, dongj@ornl.gov

Aggregation of heating, ventilation, and air conditioning (HVAC) loads can provide reserves to absorb volatile renewable energy, especially solar photo-voltaic (PV) generation. In this paper, we decide HVAC control schedules under uncertain PV generation, using a distributionally robust chance-constrained (DRCC) building load control model under two typical ambiguity sets: the moment-based and Wasserstein ambiguity sets. We derive mixed integer linear programming (MILP) reformulations for DRCC problems under both sets. Especially, for the Wasserstein ambiguity set, we utilize the right-hand side (RHS) uncertainty to derive a more compact MILP reformulation than the commonly known MILP reformulations with big-M constants. All the results also apply to general individual chance constraints with RHS uncertainty. Furthermore, we propose an adjustable chance-constrained variant to achieve trade-off between the operational risk and costs. We derive MILP reformulations under the Wasserstein ambiguity set and second-order conic programming (SOCP) reformulations under the moment-based set. Using real-world data, we conduct computational studies to demonstrate the efficiency of the solution approaches and the effectiveness of the solutions.

Key words: Building Load Control, Renewable Engergy, Distributionally Robust Optimization, Chance-Constrained Program, Binary Program

With growing environmental consciousness and government regulations, renewable energy sources (RESs) are expected to account for 29% of the total electricity consumption by 2040 (Conti et al. 2016). Given that the renewable energy generally cannot adjust their output to reflect changes of demand, higher penetration of renewable energy may cause electrical supply and demand

imbalance issues and can be challenging with variability in output and stress on electricity grids' balance, e.g., network frequency and voltage stability (Teodorescu et al. 2011).

With the advanced development of smart sensing and control technologies, one solution is utilizing heating, ventilation, and air conditioning (HVAC) systems as grid-responsive flexible load resource, i.e., demand response. Given their large amount of power consumption, enormous thermal mass and considerable resistances, the flexible HVAC loads can be employed as virtual storage resources to compensate high frequent fluctuations in renewable energy such as solar photo-voltaic (PV) (Yin et al. 2016).

In Dong et al. (2017, 2018), they study the problem of using aggregated HVAC systems to absorb solar PV generation. However, the inherent uncertainties of the problem are ignored in their deterministic models, such as uncertainties of the thermal controlled loads (TCLs) and renewable resources, which are mainly determined by factors of weather and consumer behavior (Zhang et al. 2018a). The uncertainties can be further intensified by missing samples and low resolution information in HVAC data collection (Wijayasekara and Manic 2015, Žáčeková et al. 2014). In this paper, we take the uncertainties into consideration by employing distributionally robust chance-constrained (DRCC) programs.

0.1. Relevant Literature

The aggregated HVAC loads as a virtual storage have become a key player in providing grid demand-responsive services including load balancing (see, e.g., Lu 2012, Dong et al. 2017, Barooah 2019, Wang et al. 2020). Hao et al. (2014) provide a virtual storage model to characterize aggregate energy flexibility from building loads. It is followed by virtual storage model identification and flexibility quantification in Hughes et al. (2015) and Stinner et al. (2016), respectively. With the support of home energy management systems (HEMSs), distribution system operators (DSOs) can connect with customers (e.g., using virtual storage model via aggregated HVAC loads) to realize system-wide control objectives, e.g., demand response. Deterministic optimization models have been proposed to orchestrate the aggregated virtual storage devices (see, e.g., Hao et al.

2017, Dong et al. 2018). In addition to the scalability and privacy issues, residential demand response programs also confront the challenges of handling uncertain parameters, e.g., uncertainties of weather and consumer behavior. To consider the impacts of forecasting errors, both robust optimization and stochastic programming techniques have been introduced to account for modeling disturbance uncertainties (see, e.g., Chen et al. 2012, Nguyen and Le 2014, Zhang et al. 2019, Kocaman et al. 2020). For example, Diekerhof et al. (2017) schedule flexible devices to reduce peak loads and customers bills under weather and occupancy uncertainties. They propose a distributed robust optimization framework to hedge against the worst-case scenario. Lu et al. (2020) apply robust optimization to maintain thermal comfort in heat and electricity integrated energy systems. Nguyen et al. (2014) propose a two-stage stochastic program which uses HVAC loads to smooth out the power fluctuation of a wind farm and/or a solar farm. Alhaider et al. (2016) further take sizing decisions of PV systems and decisions of battery energy storage systems into account, and formulate a two-stage stochastic integer linear program.

Recently, distributionally robust optimization (DRO) techniques have gained wide interest. Instead of assuming a specific probability distribution of the system uncertainties as in stochastic programming, the DRO approaches consider a family of probability distributions with prior knowledge of the uncertainties, termed as ambiguity set. The DRO approaches have been applied to many problems in power systems, such as energy storage operation (see, e.g., Yang 2019), optimal power flow (see, e.g., Zhang et al. 2016, Duan et al. 2018), and unit commitment (see, e.g., Zhao and Jiang 2018). Two typical groups of the ambiguity sets employed in DRO are moment-based (e.g., Delage and Ye 2010) and distance-based (e.g., Wasserstein metric Esfahani and Kuhn 2018) ambiguity sets. For example, considering a moment-based ambiguity set, Zhang et al. (2019) employ a DRCC program to enable more effective use of uncertain renewables with HVAC systems. A similar formulation has been proposed in Guo et al. (2020) to solve optimal pump coordination in water distribution networks under uncertain water demand. They consider a distributionally robust two-stage stochastic program under a Wasserstein ambiguity set. The stochastic model predictive control (MPC), an approach for energy efficiency in HVAC units (Dong et al. 2018), has

been considered with distributionally robust chance constraints in Mark and Liu (2020). They use conditional value-at-risk (CVaR) to approximate the chance constraints.

Another stream of research relevant to this paper is on adjustable chance constraints. Instead of considering a predetermined (fixed) risk level for chance constraints, decision makers can be interested in balancing between the risk level and operational costs by varying the risk level. The adjustable chance constrained models treat the risk levels as decision variables, which have been applied to various problems, such as metal melting (Evers 1967), flexible ramping capacity (Wang et al. 2018), power dispatch (Qiu et al. 2016, Ma et al. 2019), portfolio optimization (Lejeune and Shen 2016), and humanitarian relief network design (Elçi et al. 2018). Wang et al. (2018) and Evers (1967) assume that the inverse of the cumulative distribution is known, which, however, is not always accessible. Qiu et al. (2016) approximate the chance constraint by the sample average approximation and transform the problem to a mixed-integer program. When the uncertainty only happens on the right-hand side, assuming a discrete distribution, Shen (2014) proposes a mixed integer linear programming (MILP) reformulation based on p-efficient point using a special ordered set of type 1 (SOS1) constraint. Along the same vein, Elçi et al. (2018) propose an alternative MILP using a knapsack inequality which yields an equivalent linear programming relaxation as the one in Shen (2014). All the research above works on individual chance constraint. For joint chance constraints, Bonferroni approximation is one classical approximation, which enforces individual chance constraints with variable risk levels and bounds on the sum of the risk levels. Xie et al. (2019) study the Bonferroni approximation of distributionally robust joint chance constraints under a moment-based ambiguity set which matches the exact mean and covariance. Ma et al. (2019) apply a similar joint chance constraint, which further requires unimodality, to a power dispatch problem with do-not-exceed limits.

0.2. Summary of Main Contributions

In this paper, in addition to the moment-based ambiguity set used in the prior work of Zhang et al. (2019), we further consider DRCC programs under the Wasserstein ambiguity set. In particular,

by exploiting the right-hand-side (RHS) uncertainty, we derive an MILP reformulation based on the conditional value-at-risk (CVaR) interpretation for DR chance constraints pointed out by Xie (2019), Chen et al. (2018). Recently, based on the CVaR (primal) interpretation, Ho-Nguyen et al. (2021) provide an MILP reformulations for joint DRCC programs with RHS uncertainty. From the primal perspective, CVaR is a conditional expectation at the tail of a distribution; while the dual representation further indicates that CVaR is a weighted sum of the least favorable outcomes. Our results are built based on the dual perspective by deriving the weights of the least favorable outcomes. Moreover, to better balance the operational cost and PV utilization, we propose an adjustable chance-constrained formulation that treats the risk level of chance constraints as a decision variable rather than a given (fixed) parameter in the DRCC formulations. We summarize our contributions as follows:

- 1. We formulate the building load control (BLC) problem of HVAC units using DRCC optimization under two types of ambiguity sets: moment-based and Wasserstein ambiguity sets in Section 2. We also propose their variants with adjustable chance constraints to balance operational cost and performance in Section 3.
- 2. We provide exact reformulations for the DRCC and the adjustable DRCC formulations (with binary decision variables). Specifically, under the Wasserstein ambiguity set, we derive exact MILP reformulations for both DRCC and its adjustable variant. Under the moment-based ambiguity set, DRCC yields an MILP reformulation, while solving the adjustable DRCC is equivalent to solving two second-order conic programs (SOCPs). All the results for DRCC models hold for general individual DR chance constraints with RHS uncertainty (even with continuous decision variables), while the results for the adjustable variants hold for general adjustable individual binary DR chance constraint with RHS uncertainty.
- 3. We conduct computational tests on various instances and demonstrate the efficiency and effectiveness of the proposed reformulations via real-world data in Sections 4–6.

The remainder of the paper is organized as follows. Section 1 presents the mathematical formulations of the deterministic and stochastic chance-constrained BLC problems. In Sections 2–3, we

present the DRCC models and their adjustable variants, and derive exact reformulations under both the moment-based and Wasserstein ambiguity sets. In Sections 4–6, we conduct extensive numerical studies on both non-adjustable DRCC models and adjustable chance-constrained models. Finally, we draw conclusions in Section 7.

1. Model Formulation

The BLC problem utilizes an aggregated HVAC load of N_{HVAC} units, e.g., buildings, to absorb the solar PV generation (collected from N_{PV} PV panels) locally while delicately maintaining desired indoor temperature for each unit throughout the day. We discretize the day-time duration into N_p periods with a time interval of Δt (e.g., 10 minutes). For each period $t = 1, ..., N_p$, denote a binary decision variable $u_{t,\ell} \in \{0,1\}$ for HVAC unit ℓ to indicate its scheduled mode: if $u_{t,\ell} = 1$, ON; otherwise $u_{t,\ell} = 0$, OFF.

For each HVAC unit, to characterize the dynamics of room temperature and outdoor temperature, we consider a widely used building thermal model (see e.g., Mathieu et al. 2013), where the system state is the room temperature T, the system input is HVAC ON/OFF status, $Mode_{\rm HVAC}$, and the system disturbances include outdoor temperature $T_{\rm out}$ and solar irradiance $Q_{\rm out}$. Based on the building thermal model, a continuous-time linear time invariant (LTI) system for each HVAC unit in the state-space form is as follows.

$$\dot{T} = \frac{1}{RC}T_{\text{out}} + \frac{1}{RC}T + \frac{1}{C}Q_{\text{out}} + \frac{Mode_{\text{HVAC}}}{C}Q_{\text{HVAC}},\tag{1}$$

where R is the building's thermal resistance, C is the building's thermal capacity, and $Q_{\rm HVAC}$ is cooling capacity of the building. These parameters can be estimated following standard building energy modeling techniques, Resistance-Capacitance (RC) model (Belić et al. 2016, Cui et al. 2019), in particular. Such continuous-time LTI model is further converted into a discrete-time model using various techniques including the Zero-Order Hold (ZOH) method. In this paper, for each individual building $\ell=1,\ldots,N_{\rm HVAC}$, we consider a discrete-time building thermal model with a sampling interval of Δt as

$$x_{t,\ell} = A_{\ell} x_{t-1,\ell} + B_{\ell} u_{t,\ell} + G_{\ell} v_{\ell}, \tag{2}$$

where $x_{t,\ell}$ is the room temperature of period t, $u_{t,\ell}$ is the binary mode decision variable, v_{ℓ} is the system disturbance, and the parameters $A_{\ell}, B_{\ell}, G_{\ell}$ can be computed from the continuous-time model (1).

In this study, we focus on the single-period models, where we solve for the optimal ON/OFF mode decisions at the current period given an initial room temperature resulted from previous periods' decisions. To solve the control problem for all N_p periods, we sequentially solve N_p small optimization problems, each for one period. The problem can also be formulated as a multi-period model, which solves one monolithic optimization problem for all the mode decision variables over N_p periods. In our preliminary results of Zhang et al. (2019), via extensive computational studies, we demonstrate that the multi-period models have similar solutions as those of single-period models using DRCC approaches under the moment-based ambiguity set. However, the multi-period models can suffer from computational difficulty especially for large-sized problems. Therefore, in this paper, we focus on the single-period models. For the rest of this section, we present two optimization formulations of the single-period models: a deterministic formulation, which assumes that the solar PV generation is deterministic and perfectly known, and a chance-constrained formulation, which assumes the PV generation is stochastic.

1.1. Deterministic Formulation

At period t, we denote $x_t = (x_{t,\ell}, \ \ell = 1, \dots, N_{\text{HVAC}})^{\top}$ the auxiliary decision vector of room temperature of N_{HVAC} buildings, and denote $u_t = (u_{t,\ell}, \ \ell = 1, \dots, N_{\text{HVAC}})^{\top}$ the mode vector of ON/OFF decisions of N_{HVAC} buildings. For building ℓ in the ON mode, the energy consumption of one period is P_{ℓ} . We assume that the solar PV generation at period t is perfectly known as $P_{\text{PV},t} \in \mathbb{R}^{N_{\text{PV}}}$. At time t, given an initial room temperature $x_{t-1,\ell}$, $\ell = 1, \dots, N_{\text{HVAC}}$, the BLC problem can be formulated as the following MILP (Dong et al. 2018, Zhang et al. 2019).

$$\min_{u_{t},\eta,\beta_{t,\ell},x_{t,\ell}} c_{\text{sys}} \sum_{\ell=1}^{N_{\text{HVAC}}} \beta_{t,\ell} + c_{\text{switch}} \sum_{\ell=1}^{N_{\text{HVAC}}} u_{t,\ell} + c_{\text{PV}} \eta$$
s.t. (2)

$$-\eta \le \sum_{\ell=1}^{N_{\text{HVAC}}} P_{\ell} u_{t,\ell} - \sum_{i=1}^{N_{\text{PV}}} P_{\text{PV},t,i} \le \eta$$
 (3b)

$$-\beta_{t,\ell} \le x_{t,\ell} - x_{\text{ref}} \le \beta_{t,\ell}, \ \ell = 1, \dots, N_{\text{HVAC}}$$
(3c)

$$x_{\min} \le x_{t,\ell} \le x_{\max}, \ \ell = 1, \dots, N_{\text{HVAC}}$$
 (3d)

$$u_t \in \{0,1\}^{N_{\text{HVAC}}},\tag{3e}$$

where, in the objective, auxiliary variable $\beta_{t,\ell} = |x_{t,\ell} - x_{\text{ref}}|$ denotes the room temperature deviation from the set-point x_{ref} and $\eta = |\sum_{\ell=1}^{N_{\text{HVAC}}} P_\ell u_{t,\ell} - \sum_{i=1}^{N_{\text{PV}}} P_{\text{PV},t,i}|$ denotes the signal deviation between the total control signal (of all N_{HVAC} buildings) and the total PV signal (of all N_{PV} PV panels). The objective (3a) minimizes the total penalty cost of i) discomfort (indicated by the room temperature deviation), ii) switching cycles, and iii) PV tracking error, with unit cost parameters $c_{\text{sys}}, c_{\text{switch}}, c_{\text{PV}}$. Constraints (3d) require that the room temperature $x_{t,\ell}$ is maintained in the comfort band $[x_{\text{min}}, x_{\text{max}}]$ for building $\ell = 1, \dots, N_{\text{HVAC}}$. The last constraint (3e) enforces binary decision u_t .

1.2. Chance-Constrained Formulation

An accurate prediction of the solar PV output $P_{PV,t}$ is critical to the performance of the deterministic formulation (3). However, in practice, a good prediction of the PV output may not be available, due to the fluctuating nature of solar energy, which can be introduced by cloud shadows, wind speed, and other factors, and thus can be uncertain. In this section, we introduce a chance-constrained formulation to take into account uncertain PV output.

Instead of penalizing the signal deviation η in the objective to enforce all PV generation being consumed, the chance-constrained formulation (4) employs a soft constraint (4b), the chance constraint to ensures that, with a high probability, the solar PV output is consumed by the HVAC fleet. The chance-constrained formulation is

$$\min_{u_t, \beta_{t,\ell}, x_{t,\ell}} c_{\text{sys}} \sum_{\ell=1}^{N_{\text{HVAC}}} \beta_{t,\ell} + c_{\text{switch}} \sum_{\ell=1}^{N_{\text{HVAC}}} u_{t,\ell}$$
(4a)

s.t.
$$\mathbb{P}\left(\sum_{\ell=1}^{N_{\text{HVAC}}} P_{\ell} u_{t,\ell} - \sum_{i=1}^{N_{\text{PV}}} \widetilde{P}_{\text{PV},t,i} \ge 0\right) \ge 1 - \alpha_t$$
 (4b)

where $\widetilde{P}_{\mathrm{PV},t,i}$ denotes the uncertain PV generation at period t of panel i. Constraint (4b) ensures that the PV generation is absorbed by the HVAC fleet with probability $1 - \alpha_t$. The risk level $\alpha_t \in (0,1)$ is predefined and reflects system operator's risk preference, usually a small number.

To solve the chance-constrained model, we employ the Sample Average Approximation (SAA) approach (see, e.g., Luedtke and Ahmed 2008) to derive bounds and obtain feasible solutions. Using the Monte Carlo sampling method, we generate a set of finite samples of the uncertainty $\tilde{P}_{\text{PV},t}$. and enforce $\sum_{\ell=1}^{N_{\text{HVAC}}} P_{\ell} u_{t,\ell} - \sum_{i=1}^{N_{\text{PV}}} \tilde{P}_{\text{PV},t,i} \geq 0$ for sufficiently many samples.

Specifically, we generate N i.i.d. scenarios of the uncertain PV output $\widetilde{P}_{PV,t}$, denoted by $P_{PV,t}^1, \ldots, P_{PV,t}^N$. Each scenario $P_{PV,t}^n$ is associated with a probability $p_{t,n} \geq 0$, such that $\sum_{n=1}^N p_{t,n} = 1$. For each scenario n, we associate a binary variable ρ_n such that $\rho_n = 0$ indicates

$$\sum_{\ell=1}^{N_{\text{HVAC}}} P_{\ell} u_{t,\ell} - \sum_{i=1}^{N_{\text{PV}}} P_{\text{PV},t,i}^n \ge 0$$
 (5)

and when $\rho_n = 1$, constraint (5) is relaxed and can be violated. The chance constraint (4b) is approximated (see, e.g., Ruszczyński 2002) by

$$\sum_{\ell=1}^{N_{\text{HVAC}}} P_{\ell} u_{t,\ell} - \sum_{i=1}^{N_{\text{PV}}} P_{\text{PV},t,i}^{n} \ge -M \rho_{n}, \ n = 1, \dots, N$$
 (6a)

$$\sum_{n=1}^{N} p_n \rho_n \le \alpha_t \tag{6b}$$

$$\rho_n \in \{0, 1\}, \ n = 1, \dots, N,$$
 (6c)

where M is a big-M coefficient. Constraint (6b) ensures that the probability of violating (5) is no more than α_t . By replacing the chance constraint (4b) with (6a)–(6c), we obtain an MILP approximation of the chance-constrained model (4).

2. DRCC Formulations

In the stochastic chance-constrained formulation (4), full knowledge of the PV's probability distribution is required. However, an accurate probability distribution can be challenging to obtain especially when the underlying distribution (while ambiguous) is time-varying. As a consequence,

the solution obtained from the chance-constrained model might be sensitive to the choice of probability distribution and thus results in poor performance. This phenomenon is called the optimizer's curse (Smith and Winkler 2006) of solving stochastic programs. To address the curse, a natural way is to employ a set of plausible probability distributions, denoted as \mathcal{D}_t , rather than assuming a specific probability distribution. Specifically, we consider the DRCC formulation as follows

$$\min_{u_t, \beta_{t,\ell}, x_{t,\ell}} c_{\text{sys}} \sum_{\ell=1}^{N_{\text{HVAC}}} \beta_{t,\ell} + c_{\text{switch}} \sum_{\ell=1}^{N_{\text{HVAC}}} u_{t,\ell}$$
 (7a)

s.t.
$$\inf_{f \in \mathcal{D}_t} \mathbb{P}\left(\sum_{\ell=1}^{N_{\text{HVAC}}} P_\ell u_{t,\ell} - \sum_{i=1}^{N_{\text{PV}}} \widetilde{P}_{\text{PV},t,i} \ge 0\right) \ge 1 - \alpha_t$$

$$(2), (3c) - (3e).$$

$$(7b)$$

Constraint (7b) ensures that the probability of absorbing the PV generation locally by the HVAC fleet is guaranteed at least $1 - \alpha_t$ for any probability distribution $f \in \mathcal{D}_t$. That is, for all probability distributions in D_t , the worst-case probability of coordinating the HVAC fleet to consume the PV generation is no less than $1 - \alpha_t$. We note that constraint (7b) is an individual DR chance constraint with RHS uncertainty.

2.1. Ambiguity Sets

One critical question of the DRCC formulation is how to choose the ambiguity set \mathcal{D}_t . A good choice of \mathcal{D}_t should take into account the characteristics of the underlying probability distribution and the tractability of the DRCC formulation. Two types of ambiguity sets have been widely studied: (i) moment-based and (ii) distance-based ambiguity sets. In this paper, we consider a moment-based ambiguity set containing moment constraints on the first- and second-order moments (see, e.g., Delage and Ye 2010) and a distance-based ambiguity set using Wasserstein metric (e.g., Esfahani and Kuhn 2018). Given a series of independent samples, $\{P_{\text{PV},t}^n\}_{n=1}^N$, sampled from the true underlying distribution of the PV generation, we consider the following two distributional ambiguity sets.

(i) Moment-based Ambiguity Set. The empirical mean and covariance matrix can be calculated as $\mu_t = \frac{1}{N} \sum_{n=1}^{N} P_{\text{PV},t}^n$, $\Sigma_t = \frac{1}{N} \sum_{n=1}^{N} (P_{\text{PV},t}^n - \mu_t) (P_{\text{PV},t}^n - \mu_t)^{\top}$. The ambiguity set based on the two moment estimates μ_t , Σ_t , first proposed by Delage and Ye (2010), is as follows.

$$\mathcal{D}_{t}^{1} = \left\{ \begin{aligned} & \mathbb{P}_{f}(\widetilde{P}_{\mathrm{PV},t} \in \mathbb{R}^{N_{\mathrm{PV}}}) = 1 \\ & f : \ (\mathbb{E}_{f}[\widetilde{P}_{\mathrm{PV},t}] - \mu_{t})^{\top} \Sigma_{t}^{-1} (\mathbb{E}_{f}[\widetilde{P}_{\mathrm{PV},t}] - \mu_{t}) \leq \gamma_{1}, \\ & \mathbb{E}_{f} \left[(\widetilde{P}_{\mathrm{PV},t} - \mu_{t}) (\widetilde{P}_{\mathrm{PV},t} - \mu_{t})^{\top} \right] \leq \gamma_{2} \Sigma_{t}, \end{aligned} \right\},$$

where $\gamma_1 \geq 0$ and $\gamma_2 \geq \max\{\gamma_1, 1\}$. The three constraints guarantee that (1) the true mean of $\widetilde{P}_{\mathrm{PV},t}$ lies in an ellipsoid centered at μ_t and (2) the true covariance of $\widetilde{P}_{\mathrm{PV},t}$ is bounded above by $\gamma_2 \Sigma_t$. The two parameters γ_1 and γ_2 reflect the system operator's tolerance of the moment and distributional ambiguity: the larger the two parameters are, the more the tolerance towards ambiguity and the more robustness of the optimal solutions are. The values of γ_1 and γ_2 depend on the samples size, support size, and confidence level (See more details in Definition 2 in Delage and Ye 2010).

(ii) Wasserstein Ambiguity Set. Given a positive radius $\delta_t > 0$, the Wasserstein ambiguity set defines a ball around the discrete empirical distribution based on the N samples, $\mathbb{P}_{\widetilde{P}_{\mathrm{PV},t}^N}\left[\widetilde{P}_{\mathrm{PV},t} = P_{\mathrm{PV},t}^n\right] = 1/N$, in the space of probability distributions as follows.

$$\mathcal{D}_t^2 = \left\{ f : \mathbb{P}_f \{ \widetilde{P}_{\mathrm{PV},t} \in \mathbb{R}^{N_{\mathrm{PV}}} \} = 1, \ W(\mathbb{P}_f, \mathbb{P}_{\widetilde{P}_{\mathrm{PV},t}}^N) \le \delta_t \right\},\,$$

where the Wasserstein distance is defined as

$$W(\mathbb{P}_1,\mathbb{P}_2) = \inf_{\mathbb{Q}} \left\{ \int_{\mathbb{R}^{N_{\text{PV}}} \times \mathbb{R}^{N_{\text{PV}}}} \|P_{\text{PV},t}^1 - P_{\text{PV},t}^2\| \mathbb{Q}(\mathrm{d}P_{\text{PV},t}^1, \mathrm{d}P_{\text{PV},t}^2) : \\ \sup_{\text{marginals } \mathbb{P}_1 \text{ and } \mathbb{P}_2, \text{ respectively} \\ \text{tively} \right\}.$$

The radius of the ambiguity set controls the degree of the conservatism of the DRCC model. If we set $\delta_t = 0$, the ambiguity set \mathcal{D}_t^2 only contains the empirical distribution and we can recover a chance-constrained model.

2.2. DRCC Reformulation under Moment-based Ambiguity Set \mathcal{D}_t^1

Let $\theta_t = \mathbf{1}^{\top} \mu_t$ and $\sigma_t = \mathbf{1}^{\top} \Sigma_t \mathbf{1}$, where $\mathbf{1} \in \mathbb{R}^{N_{\text{PV}}}$ is a vector with all ones. We follow Zhang et al. (2018b) to rewrite the DR chance constraint (7b) under the moment-based ambiguity set \mathcal{D}_t^1 as a linear constraint.

PROPOSITION 1 (Adapted from Theorem 3.2 of Zhang et al. (2018b)). The DR chance constraint (7b) under $\mathcal{D}_t = \mathcal{D}_t^1$ is equivalent to

$$\sum_{\ell=1}^{N_{HVAC}} P_{\ell} u_{t,\ell} \ge \theta_t + \Omega_t \sigma_t, \text{ where } \Omega_t = \begin{cases} \sqrt{\gamma_1} + \sqrt{(1-\alpha_t)(\gamma_2 - \gamma_1)/\alpha_t}, \ \gamma_1/\gamma_2 \le \alpha_t \\ \sqrt{\gamma_2/\alpha_t}, & \gamma_1/\gamma_2 > \alpha_t. \end{cases}$$
(8)

Instead of enforcing the DR chance constraint with the RHS uncertainty of PV generation, constraint (8) requires the total HVAC load no less than the nominal PV generation θ_t plus the product of Ω_t and its standard deviation σ_t , where the value of Ω_t is determined by the relationship of the ambiguity set parameters γ 's and the risk level α_t . Then the DRCC formulation (7) under \mathcal{D}_t^1 is equivalent to the following MILP problem.

$$\min_{u_{t},\beta_{t,\ell},x_{t,\ell}} \left\{ c_{\text{sys}} \sum_{\ell=1}^{N_{\text{HVAC}}} \beta_{t,\ell} + c_{\text{switch}} \sum_{\ell=1}^{N_{\text{HVAC}}} u_{t,\ell} : (2), (3c) - (3e), (8) \right\}.$$

2.3. DRCC Reformulations under Wasserstein Ambiguity Set \mathcal{D}_t^2

Denote the total PV output $P_{\text{total},t}^n = \mathbf{1}^{\top} P_{\text{PV},t}^n$. According to Corollary 2 in Xie (2019) (Theorem 3 in Chen et al. 2018), the DR chance constraint (7b) under the Wasserstein ambiguity set \mathcal{D}_t^2 is feasible if and only if the following constraints, with auxiliary variables γ and z_n , $n = 1, \ldots, N$, are satisfied

$$\delta_t - \alpha_t \gamma \le \frac{1}{N} \sum_{n=1}^N z_n \tag{9a}$$

$$-\max\left[\sum_{\ell=1}^{N_{\text{HVAC}}} P_{\ell} u_{t,\ell} - P_{\text{total},t}^{n}, \ 0\right] \le -z_n - \gamma, \ n = 1, \dots, N$$
(9b)

$$z_n \le 0, \ n = 1, \dots, N \tag{9c}$$

$$\gamma \ge 0.$$
 (9d)

We remark that the reformulation (9) admits a CVaR interpretation (Xie 2019), i.e.,

$$\frac{\delta}{\alpha_t} + \text{CVaR}_{1-\alpha_t} \left[-\max \left\{ \sum_{\ell=1}^{N_{\text{HVAC}}} P_\ell u_\ell - \widetilde{P}_{\text{PV}}, 0 \right\} \right] \le 0, \tag{10}$$

where
$$\text{CVaR}_{1-\alpha_t}\left[-\max\left\{\sum_{\ell=1}^{N_{\text{HVAC}}}P_\ell u_\ell - \widetilde{P}_{\text{PV}}, 0\right\}\right] = \min_{\gamma}\left\{\gamma + \frac{1}{\alpha_t}\mathbb{E}_{\mathbb{P}^N_{\tilde{P}_{\text{PV},t}}}\left[-\max\left\{\sum_{\ell=1}^{N_{\text{HVAC}}}P_\ell u_\ell - \widetilde{P}_{\text{PV}}, 0\right\} - \gamma\right]_+\right\}$$
To linearize the the nonlinear constraints (9b), we introduce big-M coefficients for $n=1,\ldots,N$,
$$M_n^1 = \max_{u_t}\left\{\left|\sum_{\ell=1}^{N_{\text{HVAC}}}P_\ell u_{t,\ell} - P_{\text{total},t}^n\right|\right\} = \max\left\{\left|\sum_{\ell=1}^{N_{\text{HVAC}}}P_\ell - P_{\text{total},t}^n\right|, P_{\text{total},t}^n\right\}.$$
 We also introduce an auxiliary variable $s_n = \max\left[\sum_{\ell=1}^{N_{\text{HVAC}}}P_\ell u_{t,\ell} - P_{\text{total},t}^n, 0\right]$ and a binary indicator variable y_n for $n=1,\ldots,N$. The constraints (9b) are equivalent to the following MILP constraints.

$$z_n + \gamma \le s_n, \ n = 1, \dots, N \tag{11a}$$

$$s_n \le \sum_{\ell=1}^{N_{\text{HVAC}}} P_{\ell} u_{t,\ell} - P_{\text{total},t}^n + M_n^1 (1 - y_n), \ n = 1, \dots, N$$
 (11b)

$$s_n \le M_n^1 y_n, \quad n = 1, \dots, N \tag{11c}$$

$$y_n \in \{0, 1\}, \ n = 1, \dots, N$$
 (11d)

$$s_n \ge 0, \ n = 1, \dots, N.$$
 (11e)

Therefore, the DRCC formulation (7) under \mathcal{D}_t^2 is reformulated as an MILP problem as follows.

$$\mathbf{MILP1:} \ \min_{u_t, \beta_{t,\ell}, x_{\ell,t}} \left\{ c_{\text{sys}} \sum_{\ell=1}^{N_{\text{HVAC}}} \beta_{t,\ell} + c_{\text{switch}} \sum_{\ell=1}^{N_{\text{HVAC}}} u_{t,\ell} \colon (2), \ (3c) - (3e), \ (9a), \ (9c) - (9d), \ (11a) - (11e) \right\}.$$

Remark 1. Reformulation (11) involves 3N constraints and N binary variables, which may pose computational challenges as N grows large.

Next, by exploiting the dual of the CVaR interpretation, we provide a more compact MILP reformulation for the DR chance constraint with only $2\lfloor \alpha_t N \rfloor + 2$ constraints and $\lfloor \alpha_t N \rfloor + 1$ binary variables. The problem size can be significantly reduced when α_t is small.

We first sort $\{P_{\text{total},t}^n\}_{n=1}^N$ such that $P_{\text{total},t}^{(1)} \geq P_{\text{total},t}^{(2)} \geq \cdots \geq P_{\text{total},t}^{(N)}$ and obtain the non-increasing permutation $\{(1),(2),\ldots,(n)\}$ of $\{1,2,\ldots,N\}$. Denote $P_{\text{total},t}^{(0)} = \sum_{\ell=1}^{N_{\text{HVAC}}} P_{\ell}$, the maximum load provided by turning on all HVAC units. We make the following assumption.

Assumption 1. $P_{total,t}^{(0)} > P_{total,t}^{(N)}$

This is a mild assumption that requires the smallest value of the solar PV generation realization smaller than the maximum HVAC load provided when all the HVAC units are ON.

THEOREM 1. Under Assumption 1, the DR chance constraint (7b) under the Wasserstein ambiguity set \mathcal{D}_t^2 is feasible if and only if the following linear constraints are feasible with auxiliary variables $a_n, h_n \in \{0,1\}, n = 1, ..., k+1$, where $k = \lfloor \alpha_t N \rfloor$.

$$\frac{1}{N} \sum_{n=1}^{k} a_n + \left(\alpha_t - \frac{k}{N}\right) a_{k+1} \ge \delta \tag{12a}$$

$$a_n \le \sum_{\ell=1}^{N_{HVAC}} P_\ell u_{t,\ell} - P_{total,t}^{(n)} + M_n^2 (1 - h_n), \ n = 1, \dots, k+1$$
 (12b)

$$a_n \le M_n h_n, \quad n = 1, \dots, k + 1 \tag{12c}$$

$$h_n \in \{0, 1\}, \ a_n \ge 0, \ n = 1, \dots, k + 1,$$
 (12d)

where M_n and M_n^2 are sufficiently large big-M constants.

Proof: According to (9), the DR chance constraint (7b) with $\mathcal{D}_t = \mathcal{D}_t^2$ is satisfied if and only if the optimal value of the following linear program is no more than $-\delta_t$.

$$\min -\frac{1}{N} \sum_{n=1}^{N} z_n - \alpha_t \gamma \tag{13a}$$

s.t.
$$-a_n \le -z_n - \gamma, \ n = 1, \dots, N$$
 (13b)

$$z_n \le 0, \ n = 1, \dots, N \tag{13c}$$

$$\gamma \ge 0,\tag{13d}$$

where

$$a_n = \max \left[\sum_{\ell=1}^{N_{\text{HVAC}}} P_\ell u_{t,\ell} - P_{\text{total},t}^{(n)}, 0 \right], \ n = 1, \dots, N.$$
 (14)

We associate dual variables $\pi_n \geq 0$, n = 1, ..., N with constraints in (13b) and obtain the dual problem as follows.

$$\max -\sum_{n=1}^{N} \pi_n a_n \tag{15a}$$

s.t.
$$\pi_n \le \frac{1}{N}, \ n = 1, \dots, N$$
 (15b)

$$\sum_{n=1}^{N} \pi_n \ge \alpha_t \tag{15c}$$

$$\pi_n \ge 0, \ n = 1, \dots, N. \tag{15d}$$

Due to strong duality, the optimal value of (15) equals to that of (13), which is $\leq -\delta_t$. Note that (15) is the dual interpretation of the CVaR (10) scaled by α_t . The problem (15) is always feasible as $0 < \alpha_t < 1$. If Assumption 1 does not hold, the DR chance constraint (7b) is infeasible. Because when the Assumption 1 does not hold, $a_n = 0, n = 1, ..., N$, for any solution of u_t and thus the optimal value of the dual problem (15) is zero. As the optimal value is more than $-\delta_t$, the DR chance constraint (7b) is then infeasible and so is the DRCC problem (7).

The problem (15) can be converted to a relaxed knapsack problem and one optimal solution that can be obtained by the greedy algorithm is

$$\pi_n = \begin{cases} \frac{1}{N}, & n = 1, \dots, k \\ \alpha_t - \frac{k}{N}, & n = k + 1 \\ 0, & n = k + 2, \dots N. \end{cases}$$

We note that π/α_t is the conditional (discrete) probability distribution of CVaR in (10). Recall that $\{(1), (2), \ldots, (n)\}$ is a permutation such that $P_{\text{total},t}^{(1)} \geq P_{\text{total},t}^{(2)} \geq \cdots \geq P_{\text{total},t}^{(N)}$, or equivalently, $0 \leq a_1 \leq a_2 \leq \cdots \leq a_N$ (because for any $n \leq m$, $\sum_{\ell=1}^{N_{\text{HVAC}}} P_\ell u_{t,\ell} - P_{\text{total},t}^{(n)} \leq \sum_{\ell=1}^{N_{\text{HVAC}}} P_\ell u_{t,\ell} - P_{\text{total},t}^{(m)}$ and thus $a_n \leq a_m$) and $k = \lfloor \alpha_t N \rfloor$ is an index such that $k/N \leq \alpha_t < (k+1)/N$. In the case where k = 0, the optimal solution is $\pi_1 = \alpha_t$ and $\pi_n = 0$, $n = 2, \ldots, N$.

Now, we obtain an equivalent reformulation of (9) as

$$-\frac{1}{N}\sum_{n=1}^{k} a_{(n)} - (\alpha_t - \frac{k}{N})a_{(k+1)} \le -\delta_t \text{ and constraint (14)}.$$
 (16)

We obtain (12a) by multiplying -1 on both sides of the first inequality above. To linearize (14), we introduce binary variables h_n for n = 1, ..., k + 1 and big-M coefficients to obtain (12b) and (12c). Now, we complete the proof. \square

The big-M coefficients in Theorem 1 can take values as $M_n^2 = P_{\text{total},t}^{(n)} - P_{\text{total},t}^{(k)}$ and $M_n = M_n^1$. Now, we obtain the second MILP reformulation of the DRCC formulation (7) under the Wasserstein ambiguity set \mathcal{D}_t^2 .

$$\mathbf{MILP2:} \ \min_{u_{t},\beta_{t,\ell},x_{t,\ell}} \left\{ c_{\text{sys}} \sum_{\ell=1}^{N_{\text{HVAC}}} \beta_{t,\ell} + c_{\text{switch}} \sum_{\ell=1}^{N_{\text{HVAC}}} u_{t,\ell} \colon \ (2), \ (3\text{c}) - (3\text{e}), \ (12\text{a}) - (12\text{d}) \right\}.$$

MILP2 can be further strengthened by the following proposition.

PROPOSITION 2. Let $k = |\alpha_t N|$.

i. If MILP2 is feasible, then

$$a_{k+1} = \sum_{\ell=1}^{N_{HVAC}} P_{\ell} u_{t,\ell} - P_{total,t}^{(k+1)}. \tag{17}$$

Thus constraints (12b) and (12c) indexed with k+1 and variable h_{k+1} can be removed from MILP2.

ii. The following inequalities are valid for MILP2.

$$h_n \le h_{n+1}, \ n = 1, \dots, k-1.$$
 (18)

Proof: For a given solution u_t , there exists a critical index j such that

$$P_{\text{total},t}^{(j)} < \sum_{\ell=1}^{N_{\text{HVAC}}} P_{\ell} u_{t,\ell} \le P_{\text{total},t}^{(j-1)}$$

and thus $a_1 = \ldots = a_{j-1} = 0 < a_j \leq \ldots \leq a_N$. In the case where for all $n = 1, \ldots, N$, $a_n > 0$, or equivalently $P_{\text{total},t}^n < \sum_{\ell=1}^{N_{\text{HVAC}}} P_\ell u_{t,\ell}$, let j = 1. According to constraints (12b)–(12c), binary variable $h_n = 1$ if only if $a_n > 0$. Given a feasible solution u_t , $h_n = 0$ for $n = 1, \ldots, j-1$ and $h_n = 1$ for $n = j, \ldots, k$. So inequalities (18) are valid.

If MILP2 is feasible, then $j \leq k+1$. Since, otherwise, the optimal value of (15) is zero which is larger than $-\delta$ and result in infeasibility. Therefore, (17) holds.

Remark 2. Theorem 1 and Proposition 2 also apply to general DR individual chance constraint with RHS uncertainty under the Wasserstein ambiguity. In particular, Theorem 1 can be extended to a joint chance constraint setting. For the sake of space, we leave this to future work. Different

from Ho-Nguyen et al. (2021) based on the CVaR interpretation, we exploit the dual perspective of the CVaR interpretation which results in fewer binary variables (Ho-Nguyen et al. (2021) require N binary variables in contrast with $\lfloor \alpha_t N \rfloor$ in MILP2). We also reveal the solution structure of the binary variables associated with samples in the individual chance constraint setting. In Section 5.1, we show the computational comparison between their reformulation and MILP2.

3. Adjustable Chance-Constrained Formulations

In the DRCC formulation (7), α_t is a pre-defined risk level, which is often chosen based on operators' experience and is usually a small number to guarantee high PV generation utilization. However, a too small α_t may result in infeasibility of the problem and can lead to high operational cost (see, e.g., Ma et al. 2019). It is challenging for the system operator to decide the value of α_t for optimally trading off between the risk and cost. Next, we consider α_t as an adjustable decision variable and modify the DRCC model (7) into the following adjustable DRCC problem.

$$\min_{u_t, \beta_{t,\ell}, x_{t,\ell}, \alpha_t} c_{\text{sys}} \sum_{\ell=1}^{N_{\text{HVAC}}} \beta_{t,\ell} + c_{\text{switch}} \sum_{\ell=1}^{N_{\text{HVAC}}} u_{t,\ell} + c_t \alpha_t$$
(19a)

s.t.
$$\inf_{f \in D_t} \mathbb{P}\left(\sum_{\ell=1}^{N_{\text{HVAC}}} P_{\ell} u_{t,\ell} - \sum_{i=1}^{N_{\text{PV}}} \widetilde{P}_{\text{PV},t,i} \ge 0\right) \ge 1 - \alpha_t$$
 (19b)

$$0 \le \alpha_t \le 1 \tag{19c}$$

$$(2), (3c) - (3e),$$

where $c_t > 0$ is the coefficient weight on the risk level α_t . If c_t is close to zero, the utilization of solar PV output is low. Section 6 presents the impact of c_t on the risk level and operational cost.

3.1. Adjustable DRCC Reformulations under Moment-based Ambiguity Set \mathcal{D}_t^1

According to (8), the choice of the coefficient Ω_t depends on the values of α_t and γ_1/γ_2 . In this section, we present 0-1 SOCP reformulations under the two cases: (i) $\gamma_1/\gamma_2 \leq \alpha_t$ and (ii) $\gamma_1/\gamma_2 > \alpha_t$.

THEOREM 2. If $\gamma_1/\gamma_2 \leq \alpha_t$, the adjustable DR chance constraint (19b) under \mathcal{D}_t^1 , or equivalently,

$$\sum_{\ell=1}^{N_{HVAC}} P_{\ell} u_{t,\ell} \ge \theta_t + \left(\sqrt{\gamma_1} + \sqrt{\frac{1 - \alpha_t}{\alpha_t} (\gamma_2 - \gamma_1)}\right) \sigma_t, \tag{20}$$

is equivalent to the following 0-1 SOCP constraints

$$d \leq P \cdot g - 2\left(\theta_t + \sigma_t \sqrt{\gamma_1}\right) \sum_{\ell=1}^{N_{HVAC}} P_\ell u_{t,\ell} + \theta_t^2 + 2\theta_t \sigma_t \sqrt{\gamma_1} + \gamma_2 \sigma_t^2$$
(21b)

$$\sum_{\ell=1}^{N_{HVAC}} P_{\ell} u_{t,\ell} \ge \theta_t + \sigma_t \sqrt{\gamma_1}$$
(21c)

$$g_{ij} \ge u_{t,i} + u_{t,j} - 1, \ g_{ij} \le u_{t,i}, \ g_{ij} \le u_{t,j}, \ g_{ij} \ge 0, \ i, j = 1, \dots, N_{HVAC},$$
 (21d)

where the operator \cdot represents the Frobenius inner product, $P \in \mathbb{R}^{N_{HVAC} \times N_{HVAC}}$ with $P_{ij} = P_i P_j$ and $q \in \mathbb{R}^{N_{HVAC} \times N_{HVAC}}$.

Proof: See Appendix A in the online supplement. \square

Theorem 3. If $\gamma_1/\gamma_2 > \alpha_t$, the adjustable DR chance constraint (19b), or equivalently,

$$\sum_{\ell=1}^{N_{HVAC}} P_{\ell} u_{t,\ell} \ge \theta_t + \sqrt{\frac{\gamma_2}{\alpha_t}} \sigma_t, \tag{22}$$

is equivalent to the following 0-1 SOCP constraints

$$\sum_{\ell=1}^{N_{HVAC}} P_{\ell} u_{t,\ell} \ge \theta_t + \phi \sigma_t \sqrt{\gamma_2}$$
 (23a)

$$\alpha_t + \phi \ge \left\| \begin{array}{c} \alpha_t - \phi \\ 2q \end{array} \right\| \tag{23b}$$

$$\phi \ge w^2 \tag{23c}$$

$$q + w \ge \begin{vmatrix} q - w \\ 2 \end{vmatrix}. \tag{23d}$$

Proof: See Appendix B in the online supplement. \square

Therefore, to solve the adjustable DRCC model (19) under the moment-based ambiguity set \mathcal{D}_t^1 , we solve the following two 0-1 SOCP problems, separately.

SOCP1:
$$\min_{u_t, \beta_{t,\ell}, x_{t,\ell}, \alpha_t} \left\{ c_{\text{sys}} \sum_{\ell=1}^{N_{\text{HVAC}}} \beta_{t,\ell} + c_{\text{switch}} \sum_{\ell=1}^{N_{\text{HVAC}}} u_{t,\ell} + c_t \alpha_t : 1 \ge \alpha_t \ge \frac{\gamma_1}{\gamma_2}, (2), (3c) - (3e), (21a) - (21d) \right\},$$

$$\mathbf{SOCP2:} \ \min_{u_t, \beta_{t,\ell}, x_{t,\ell}, \alpha_t} \left\{ c_{\text{sys}} \sum_{\ell=1}^{N_{\text{HVAC}}} \beta_{t,\ell} + c_{\text{switch}} \sum_{\ell=1}^{N_{\text{HVAC}}} u_{t,\ell} + c_t \alpha_t : \ 0 \leq \alpha_t \leq \frac{\gamma_1}{\gamma_2}, \ (2), \ (3c) - (3e), \ (23a) - (23d) \right\}.$$

After obtaining the two optimal values, we compare them and let the solution with the higher optimal value be the optimal solution to the adjustable DRCC model (19).

Note that the reformulation SOCP1 incorporates N_{HVAC}^2 auxiliary variables g_{ij} , $i, j = 1, \dots, N_{\text{HVAC}}$, which can result in computational burden when N_{HVAC} is large. Below, we present a more compact approximation that incorporates only four auxiliary variables if $\gamma_1/\gamma_2 \leq \alpha_t \leq 0.75$.

THEOREM 4. if $\gamma_1/\gamma_2 \le \alpha_t \le 0.75$, the adjustable DR chance constraint (19b) is outer approximated by the following 0-1 SOCP constraints

$$\sum_{\ell=1}^{N_{HVAC}} P_{\ell} u_{t,\ell} \ge \theta_t + \left(\sqrt{\gamma_1} + r\sqrt{\gamma_2 - \gamma_1}\right) \sigma_t \tag{24a}$$

$$2r \ge \phi \tag{24b}$$

$$\alpha_t + \phi \ge \left\| \begin{array}{c} \alpha_t - \phi \\ 2q \end{array} \right\| \tag{24c}$$

$$q + w \ge \begin{vmatrix} q - w \\ 2 \end{vmatrix} \tag{24d}$$

$$\phi \ge w^2. \tag{24e}$$

Proof: See Appendix C in the online supplement. \square

Therefore, when $\gamma_1/\gamma_2 \le \alpha_t \le 0.75$, to solve the adjustable DRCC model (19) under the moment-based ambiguity set, we can implement a branch-and-cut algorithm, which solves the following 0-1 SOCP problem.

$$\mathbf{SOCP3:} \ \min_{u_{t},\beta_{t,\ell},x_{t,\ell},\alpha_{t}} \left\{ c_{\mathrm{sys}} \sum_{\ell=1}^{N_{\mathrm{HVAC}}} \beta_{t,\ell} + c_{\mathrm{switch}} \sum_{\ell=1}^{N_{\mathrm{HVAC}}} u_{t,\ell} + c_{t} \alpha_{t} : \ 0.75 \geq \alpha_{t} \geq \frac{\gamma_{1}}{\gamma_{2}}, \ (2), \ (3\mathrm{c}) - (3\mathrm{e}), \ (24\mathrm{a}) - (24\mathrm{e}) \right\}.$$

At each iteration, obtaining the current solution $(\hat{\alpha}_t, \hat{r}, \hat{u}_t)$, if constraint (36) in the online appendix C: $r \geq \sqrt{(1-\alpha_t)/\alpha_t}$, is satisfied, we claim that $(\hat{\alpha}_t, \hat{r}, \hat{u}_t)$ is optimal. Otherwise, we generate the following supporting hyperplane as a valid inequality.

$$r \ge \left(-\frac{1}{2} (1 - \hat{\alpha}_t)^{-\frac{1}{2}} \hat{\alpha}_t^{-\frac{3}{2}} \right) \alpha_t + (1 - \hat{\alpha}_t)^{-\frac{1}{2}} \hat{\alpha}_t^{-\frac{1}{2}} (\frac{3}{2} - \hat{\alpha}_t).$$

If the decision maker chooses to only consider α_t such that $0 \le \alpha_t \le 0.75$ for the adjustable DRCC model, he first solves SOCP2 for $0 \le \alpha_t \le \gamma_1/\gamma_2$ and implement the branch-and-cut algorithm for $\gamma_1/\gamma_2 \le \alpha_t \le 0.75$. Then comparing the two optimal values, let the solution with the higher optimal value be the optimal solution to the adjustable DRCC model.

3.2. Adjustable DRCC Reformulations under Wasserstein Ambiguity Set \mathcal{D}_t^2

In the section, we first show that the adjustable DRCC model under the Wasserstein ambiguity set \mathcal{D}_t^2 can be reformulated as a 0-1 MILP formulation with big-M coefficients based on the MILP1. Then we present a big-M free MILP reformulation by exploiting the RHS uncertainty.

We denote $Z = \{u_t : (9a) - (9d)\}$ the feasible region (see Section 2.3) described by the DR chance constraint (7b) under Wasserstein ambiguity set \mathcal{D}_t^2 . Now, we consider the risk level α_t as a decision variable in the adjustable formulation. The product $\alpha_t \gamma$ in (9a) becomes a bilinear term. In the following proposition, we derive an equivalent set to Z by eliminating the bilinear term.

Proposition 3. The set Z is equivalent to the following set:

$$Z_1 = \left\{ u_t : \ \delta_t \lambda - \alpha_t \le \frac{1}{N} \sum_{n=1}^N z_n \right\}$$
 (25a)

$$-\max\left[\sum_{\ell=1}^{N_{HVAC}} P_{\ell} \lambda u_{t,\ell} - P_{total,t}^{n} \lambda, \ 0\right] \le -z_n - 1, \ n = 1, \dots, N$$
 (25b)

$$\lambda \ge 0, \ z_n \le 0, \ n = 1, \dots, N$$
 (25c)

Proof: See appendix D in the online supplement. \square

By introducing suitable big-M coefficients M_n^3 , n = 1, ..., N, the set Z_1 can be further reformulated as a mixed integer set below.

$$Z_1 = \left\{ u_t : \ \delta_t \lambda - \alpha_t \le \frac{1}{N} \sum_{n=1}^N z_n \right\}$$
 (26a)

$$z_n + 1 \le s_n, \ n = 1, \dots, N$$
 (26b)

$$s_n \le \sum_{\ell=1}^{N_{\text{HVAC}}} P_{\ell} \lambda u_{t,\ell} - P_{total,t}^n \lambda + M_n^3 (1 - y_n), \ n = 1, \dots, N$$
 (26c)

$$s_n \le M_n^3 y_n, \ n = 1, \dots, N \tag{26d}$$

$$\lambda \ge 0, \ s_n \ge 0, \ z_n \le 0, \ y_n \in \{0, 1\}, \ n = 1, \dots, N$$
 (26e)

We denote $w_{t,\ell} := \lambda u_{t,\ell}$ and constraint (26c) becomes

$$s_n \le \sum_{\ell=1}^{N_{\text{HVAC}}} P_{\ell} w_{t,\ell} - P_{total,t}^n \lambda + M_n^3 (1 - y_n), \ n = 1, \dots, N.$$
 (27)

According to the McCormick inequalities, we introduce the following linear constraints

$$w_{t,\ell} \ge 0, \ w_{t,\ell} \ge \lambda - (1 - u_{t,\ell})\lambda^{\mathrm{U}}, \ w_{t,\ell} \le \lambda^{\mathrm{U}} u_{t,\ell}, \ w_{t,\ell} \le \lambda,$$
 (28)

where λ^{U} is an upper bound of λ . Therefore, the adjustable DRCC model (19) under the Wasserstein ambiguity set is equivalent to the following 0-1 MILP formulation.

MILP3:

$$\min_{u_{t},\beta_{t,\ell},x_{t,\ell},\alpha_{t}} \left\{ c_{\text{sys}} \sum_{\ell=1}^{N_{\text{HVAC}}} \beta_{t,\ell} + c_{\text{switch}} \sum_{\ell=1}^{N_{\text{HVAC}}} u_{t,\ell} + c_{t}\alpha_{t} : (2), (3c) - (3e), (26a), (26b), (26d) - (26e), (27), (28), (19c) \right\}.$$

MILP3 is, however, difficult to solve in certain cases, according to Xie (2019) and Chen et al. (2018). A bad choice of too large values for the two big-M parameters (M_n^3 and λ^U) may lead to weak linear relaxations and thus can be detrimental to efficient computation. Taking into account the RHS uncertainty exploited in Theorem 1 and Proposition 2, next, we derive a big-M free reformulation.

THEOREM 5. Under Assumption 1, the DR chance constraint (19b) under the Wasserstein ambiguity set $\mathcal{D}_t = \mathcal{D}_t^2$ is feasible if and only if the following MILP constraints with auxiliary variables $\Delta_{jk} \in \{0,1\}, \varepsilon_{jk} \in \mathbb{R}, \tau_{\ell jk} \in \mathbb{R}, \sigma_{\ell jk} \in \mathbb{R} \text{ are feasible.}$

$$\sum_{j=1}^{N} \sum_{k=j-1}^{N-1} \left[-\frac{1}{N} \sum_{i=j}^{k} \left(P_{\text{total},t}^{(k+1)} - P_{\text{total},t}^{(i)} \right) \Delta_{jk} - \sum_{\ell=1}^{N_{HVAC}} P_{\ell} \left(o_{\ell jk} - \frac{j-1}{N} \tau_{\ell jk} \right) + P_{\text{total},t}^{(k+1)} \left(\varepsilon_{jk} - \frac{j-1}{N} \Delta_{jk} \right) \right] \le -\delta_{t} (29a)$$

$$\sum_{i=1}^{N} \sum_{k=i-1}^{N-1} \Delta_{jk} = 1 \tag{29b}$$

$$\sum_{j=1}^{N} \sum_{k=j-1}^{N-1} k \Delta_{jk} \le \sum_{j=1}^{N} \alpha_t N \le \sum_{j=1}^{N} \sum_{k=j-1}^{N-1} (k+1) \Delta_{jk}$$
(29c)

$$\sum_{j=1}^{N} \sum_{k=j-1}^{N-1} P_{total,t}^{(j)} \Delta_{jk} \le \sum_{\ell=1}^{N} P_{\ell} u_{t,\ell} \le \sum_{j=1}^{N} \sum_{k=j-1}^{N-1} P_{total,t}^{(j-1)} \Delta_{jk}$$
(29d)

$$\varepsilon_{jk} \le \Delta_{jk}, \ \varepsilon_{jk} \le \alpha_t, \ \varepsilon_{jk} \ge \alpha_t + \Delta_{jk} - 1, \ \varepsilon_{jk} \ge 0, \ 0 \le j - 1 \le k \le N - 1$$
 (29e)

$$o_{\ell jk} \le \varepsilon_{jk}, \ o_{\ell jk} \le u_{t,\ell}, \ o_{\ell jk} \ge \varepsilon_{jk} + u_{\ell} - 1, \ o_{\ell jk} \ge 0, \ 0 \le j - 1 \le k \le N - 1, \ 1 \le \ell \le N_{HVAC}$$

$$(29f)$$

$$\tau_{\ell j k} \le \Delta_{j k}, \ \tau_{\ell j k} \le u_{t, \ell}, \ \tau_{\ell j k} \ge \Delta_{j k} + u_{\ell} - 1, \ \tau_{\ell j k} \ge 0, \ 0 \le j - 1 \le k \le N - 1, \ 1 \le \ell \le N_{HVAC}$$

$$(29g)$$

$$\Delta_{jk} \in \{0,1\}, \ 0 \le j-1 \le k \le N-1.$$
 (29h)

Proof: See Appendix E in the online supplement. \square

The big-M free MILP reformulation of the adjustable DRCC formulation (19) under the \mathcal{D}_t^2 is

$$\mathbf{MILP4:} \ \min_{u_t, \beta_{t,\ell}, x_{t,\ell}, \alpha_t} \left\{ c_{\text{sys}} \sum_{\ell=1}^{N_{\text{HVAC}}} \beta_{t,\ell} + c_{\text{switch}} \sum_{\ell=1}^{N_{\text{HVAC}}} u_{t,\ell} + c_t \alpha_t : \ (2), \ (3\text{c}) - (3\text{e}), \ (29\text{a}) - (29\text{h}), \ (19\text{c}) \right\}.$$

REMARK 3. Theorem 5 also applies to general adjustable individual DR binary chance constraints with RHS uncertainty. The MILP3 reformulation (with big-M coefficients) for the adjustable chance constraint yields 3N binary variables and $3N + 3N_{\rm HVAC} + 1$ constraints. MILP4 has N(N-1)/2 binary variables and $3N(N-1)/2 + 3N(N-1)N_{\rm HVAC} + 4$ constraints.

4. Computation Setup

We consider a fleet of $N_{\rm HVAC}=100$ identical buildings and $N_{\rm PV}=1$ PV panel for $N_p=53$ periods, every 10 minutes from 8:20 am to 5:00 pm over a day. We consider two typical weather conditions: a sunny day and a cloudy day. The PV power output data (available at https://drive.google.com/drive/folders/1ERACqKeP2yYcwzbsvgTbQ13uRqFQD4Gi?usp=sharing.) of $P_{\rm PV,t}$, as shown in Figure 1, is collected from a 13 kW PV panel located on the rooftop of the Distributed Energy Communication & Control (DECC) laboratory at Oak Ridge National Laboratory (ORNL) in Tennessee. We scale the PV output to be compatible with the aggregate of 100 residential HVAC systems (connected via a same step-down transformer). For each building,

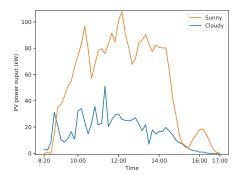


Figure 1 (Color online) PV profile

a random initial room temperature is generated by a uniform distribution between 23.10°C

and 23.15°C. The set-point $x_{\rm ref}$ is 23.0°C and the comfort band $[x_{\rm min}, x_{\rm max}]$ is [21.5, 24.5]°C. The building parameters are set as $A_{\ell} = 0.9914$, $B_{\ell} = -0.6767$, $G_{\ell} = (4.3e-5, 0.0086)^{\top}$ for $\ell = 1, \ldots, N_{\rm HVAC}$. Each HVAC system consumes 3.5 kW when it is ON. The objective costs are set as follows: $c_{\rm sys} = 1.0$, and $c_{\rm switch} = 1.0$.

In our studies we consider the two DRCC formulations, assuming unknown distributional information of the PV output generation, and the benchmark chance-constrained formulation, which are referred to as: 1. CC: stochastic chance-constrained formulation; 2. DRCC-M: DRCC under the moment-based ambiguity set; 3. DRCC-W: DRCC under the Wasserstein ambiguity set.

We generate N=100 i.i.d. samples (i.e., in-sample data) of $\widetilde{P}_{\mathrm{PV},t}$ following uniform distributions (Gaunt et al. 2017) with the mean $P_{\mathrm{PV},t}$ (shown in Figure 1) and half range of $0.15P_{\mathrm{PV},t}$ for $t=1,\ldots,N_p$. We optimize the CC model and construct the ambiguity set of the DRCC-W model by using all N=100 samples, and for DRCC-M, only 10 samples are randomly picked from the N samples to calculate the empirical mean and covariance. With the optimal schedules obtained by solving different models, we generate 10 sets of N'=1000 i.i.d. samples (i.e., out-of-sample data) from the same uniform distribution to evaluate the out-of-sample performance of each schedule. All models are computed in Python 3.7.5 using Gurobi 9.0.0. The computations are performed on a Windows 10 Pro machine with Intel(R) Core(TM) i7-8700 CPU 3.20 GHz and 16 GB memory.

5. Studies on the DRCC Models

In the DRCC-M model, we set the parameters of the moment-based ambiguity set $(\gamma_1, \gamma_2) = (0, 1)$; in the DRCC-W model, we set the radius parameter $\delta_t = 0.02$. In particular, we solve the DRCC-W model by using the two MILP formulations derived in Section 2.3. The comparison of the computation time and optimality gaps is presented in Section 5.1. In Section 5.2, we present the solution details of the three models, including the tracking performance and resulting room temperatures. In Section 5.3, we present the out-of-sample performance of optimal solutions obtained. Furthermore, we study the sensitivity of the out-of-sample performance on the in-sample data size.

5.1. CPU Time and Optimality Gaps

In this section, we show the computational performance of the two MILPs (MILP1 and MILP2 in Section 2.3) and the MILP reformulation (denoted as "MILP-H") proposed in Ho-Nguyen et al. (2021) under different sample sizes. The MILP2 formulation is strengthened by the techniques in Proposition 2. In particular, we generate 10 in-sample sets of the sunny weather following the description in Section 4, with the size of N = 100 and N = 500, respectively. For further comparing MILP2 and MILP-H, we generate 10 more in-sample sets with larger sample size N = 3000. Each instance contains $N_p = 53$ periods. Given an initial room temperature of the first period, for each instance, we sequentially solve the remaining periods by using the resulting room temperature from previous periods as an initial room temperature. The CPU time limit is 100 seconds for each period. We test various risks $1 - \alpha_t \in \{80\%, 90\%\}$ and Wasserstein radii $\delta_t \in \{0.02, 0.2\}$.

In Table 1, for each instance, we report the total CPU time of solving all 53 periods. If any period cannot be solved to optimality within the time limit, in the parentheses after the CPU times, we report the number of periods that cannot be solved within the time limit and the average optimality gaps of them. Except for $1 - \alpha_t = 90\%$, $\delta = 0.2$ and N = 100, for all other cases, the basic MILP1 has instances of which some periods cannot be solved with the time limit. In contrast, MILP-H and MILP2 solve all instances within much shorter time and (or) much smaller optimality gaps. For example, when $1 - \alpha_t = 80\%$, $\delta = 0.02$, N = 500, MILP1 solves instances using 2493.35 seconds and terminates with a 14.83% optimality gap, on average. While both MILP-H and MILP2 solve the instances optimally within 5 seconds. MILP2 is more effective when the Wasserstein ball's radius δ is small. When the radius is larger $\delta = 0.2$ with high $1 - \alpha_t = 90\%$, MILP-H yields shorter CPU times and (or) smaller gaps. If the sample size becomes larger (N=3,000), MILP-H starts to outperform HILP2 with smaller $1 - \alpha_t = 80\%$.

We also provide the average computational performance of the three MILPs when $1 - \alpha_t = \{10\%, 20\%\}$, which may be of little interest in practice, but for a fair comparison. In Table 2, MILP2 scales well when $1 - \alpha_t$ is small. While MILP1 and MILP-H require much longer time. For

Table 1 Comparison of CPU time (in seconds) and optimality gaps of high risk requirement $1-\alpha_t$

						7 6 1			
$1 - \alpha$			N = 100			N = 500		N = 3000	
	Instance	MILP1	MILP-H	MILP2	MILP1	MILP-H	MILP2	MILP-H	MILP2
	1	211.34	0.83	0.42	2522.87 (13, 14.69%)	4.43	1.76	128.38 (1, 2.92%)	32.85
	2	211.42 (1, 1.30%)	5.31	0.37	2528.31 (12, 11.16%)	2.33	1.67	88.51	33.20
	3	109.8	0.99	0.42	2390.65 (10, 15.68%)	2.84	1.60	143.16	47.51
	4	146.08	100.75~(1,~1.25%)	0.38	2387.41 (11, 9.34%)	2.56	1.67	147.98 (1, 2.99%)	32.76
	5	60.72	5.19	0.42	2365.25 (9, 18.86%)	2.82	1.68	89.44	33.37
80% 0	0.02 6	93.74	0.78	0.41	2560.81 (10, 15.53%)	4.45	1.64	56.76	34.13
	7	69.26	1.15	0.42	2653.68 (12, 21.59%)	3.29	1.70	93.66	33.95
	8	53.91	$100.70\ (1, 1.33\%)$	0.37	2411.36 (14, 8.36%)	3.01	1.60	72.63	34.38
	9	64.61	0.73	0.35	2676.71 (16, 12.29%)	2.92	1.71	82.45	33.53
	10	153.73 (1, 0.45%)	1.28	0.43	2436.43 (10, 20.84%)	2.55	1.65	153.79	33.66
	Avg.	117.46 (0.2, 0.18%)	21.77 (0.2, 0.25%)	0.40	2493.35 (11.7, 14.83%)	3.12	1.67	105.68 (0.2, 0.59%)	34.93
	1	846.05 (4, 1.60%)	0.87	0.60	2833.75 (16, 3.35%)	3.18	2.35	47.32	51.66
	2	906.48 (4, 1.67%)	0.78	0.53	3005.26 (16, 3.50%)	3.98	2.36	102.68	75.78
	3	866.27 (5, 1.28%)	0.86	0.56	3109.46 (17, 3.32%)	10.45	2.14	45.73	86.92
	4	830.88 (3, 1.12%)	0.99	0.53	2809.71 (16, 5.76%)	3.72	2.24	52.69	82.53
	5	631.79 (3, 1.13%)	0.76	0.56	3168.74 (18, 2.44%)	6.59	2.43	66.68	89.73
80% (0.2 6	843.26 (3, 1.02%)	0.83	0.57	2771.79 (14, 2.49%)	3.03	2.17	51.69	84.65
	7	874.16 (4, 1.24%)	0.92	0.57	2938.23 (16, 2.98%)	2.83	2.37	46.80	98.53
	8	835.96 (5, 1.15%)	0.98	0.58	2992.62 (20, 3.71%)	16.07	2.11	48.68	102.53
	9	823.88 (4, 1.65%)	0.85	0.54	3040.97 (17, 3.89%)	3.23	2.33	51.64	102.78
	10	688.03 (3, 1.20%)	0.98	0.62	3049.83 (18, 3.17%)	10.43	2.33	53.14	84.12
	Avg.	814.68 (3.8, 1.31%)	0.88	0.57	2972.04 (16.8, 3.46%)	6.35	2.28	56.71	85.92
	1	390.77 (2, 1.12%)	0.68	0.35	2174.93 (13, 2.15%)	1.21	0.75	13.72	9.15
	2	321.15 (2, 1.56%)	0.64	0.34	2525.91 (18, 1.81%)	1.35	0.75	15.64	9.28
	3	342.84 (2, 1.75%)	0.58	0.35	2193.18 (12, 2.96%)	1.16	0.76	8.35	9.27
	4	312.02 (1, 1.11%)	0.61	0.31	2428.54 (18, 2.55%)	1.43	0.73	10.80	8.82
	5	380.92 (3, 1.22%)	0.57	0.38	2311.06 (14, 2.17%)	1.37	0.68	13.55	9.23
0007 0		347.04 (2, 1.62%)	0.60	0.33	2144.32 (13, 1.88%)	1.19	0.75	8.61	8.80
90% 0	7	491.16 (1, 1.19%)	0.64	0.35	1958.54 (11, 1.66%)	1.07	0.74	10.01	8.67
	8	349.96 (1, 1.14%)	0.56	0.32	2304.81 (15, 2.79%)	1.33	0.65	12.45	9.13
	9	431.95 (3, 1.39%)	0.54	0.35	2098.43 (12, 1.98%)	1.21	0.77	9.58	8.64
	10	332.82 (2, 1.63%)	0.48	0.35	2355.13 (16, 1.82%)	1.28	0.80	18.37	8.49
	Avg.	370.06 (1.9, 1.37%)		0.34	2249.49 (14.2, 2.18%)	1.26	0.74	12.11	8.95
-	1 Avg.	216.17	0.44	0.44	1962.85 (8, 2.61%)	1.10	0.89	9.84	10.32
	2	220.72	0.44	0.44	1956.90 (7, 2.37%)	1.04	0.94	10.50	11.05
	3								
		214.09	0.50	0.51	2013.63 (10, 2.07%)	0.95	0.96	10.14	12.42
	4	199.31	0.45	0.47	1966.34 (10, 2.29%)	1.14	0.87	7.11	10.89
	5	239.24	0.45	0.43	1867.35 (9, 2.49%)	1.08	0.93	6.52	11.15
90% (0.2 6	285.80	0.47	0.45	1947.05 (11, 2.19%)	0.87	0.98	9.47	10.63
	7	297.24	0.43	0.55	1873.74 (7, 2.51%)	0.96	0.98	9.26	11.96
	8	236.04	0.42	0.49	1856.42 (8, 2.64%)	1.00	0.99	6.22	10.56
	9	201.77	0.42	0.47	1947.70 (10, 1.95%)	0.92	100.93 (1, 1.42%)	9.92	10.86
	10	254.37	0.42	0.45	1906.98 (10, 2.37%)	0.94	0.99	6.62	10.72
	Avg.	236.48	0.44	0.47	1929.90 (9, 2.35%)	1.00	10.95 (0.1, 0.14%)	8.56	11.06

example, when $1 - \alpha_t = 10\%$, $\delta = 0.02$, N = 100, MILP2 finishes under 5 seconds, while MILP1 uses 2379.21 seconds with a 10.41% gap and MILP-H of 195.82 seconds with a 0.09% gap. More details of each instance can be found in the online appendix G. For the moment-based ambiguity set, the computational details are in the online appendix I.

Table 2 Average CPU time (in seconds) and optimality gaps of low risk requirement $1-\alpha_t$

		N = 100				N = 500	N = 3000		
$1 - \alpha$	δ	MILP1	MILP-H	MILP2	MILP1	MILP-H	MILP2	MILP-H	MILP2
1007	0.02	80.31 (0.5, 0.17%)	8.60	0.84	2379.21 (6.9, 10.41%)	195.82 (0.2, 0.09%)	4.42	2205.50 (17.6, 4.54%)	53.67 (0.1, 0.04%)
10%	0.2	309.28 (1.8, 0.38%)	187.39 (1.5, 0.35%)	3.97	3199.71 (11.9, 20.31%)	$387.83\ (2, 0.39\%)$	10.01	2029.92 (14.9, 4.58%)	$247.49\ (1.3,\ 0.27\%)$
~	0.02	113.34 (0.7, 0.16%)	29.36 (0.2, 0.06%)	0.86	2979.62 (13.9, 26.00%)	186.22 (0.2, 0.06%)	14.70 (0.1, 0.01%)	2029.92 (14.9, 4.58%)	35.54
20%	0.2	345.01 (1.1, 0.36%)	25.9	1.58	3443.04 (12.9, 25.22%)	268.21 (0.6, 0.22%)	53.04 (0.3, 0.06%)	3388.08 (27.3, 4.06%)	212.76 (1.2, 0.34%)

5.2. Tracking Performance and Room Temperatures

In this section, we present the results under the sunny weather condition and the results for the cloudy weather condition are in the online appendix J. For the sunny weather, we solve three models for all N_p periods under the sunny weather condition with $N_{\text{HVAC}} = 100$ HVAC units. For the cloudy weather, as the PV generation is relatively lower than that of the sunny day (as shown in Figure 1), fewer number of HVAC units are enrolled to keep the total consumption compatible with the magnitude of the local PV generation (Dong et al. 2018). We remark that our model is flexible to incorporate fleet sizing decisions based on the nameplate capacity of HVAC devices and local solar PV generation scales. The details are in the online appendix F.

We present the overall tracking performance under sunny weather using 100 ON/OFF HVAC devices, i.e., $\sum_{j=1}^{N_{\text{HVAC}}} P_j u_{t,j}$, $t = 1, ..., N_p$ of the three models in Figure 2a. The shaded blue areas in the background is the plot of 100 PV generation samples used for solving the models. Overall, all three models track the PV generation well. Most of the periods, the two DRCC models provide higher HVAC loads than the stochastic CC model given that the DRCC models take into account ambiguous probability distributions and thus the solutions are more conservative. The DRCC-M model yields higher HVAC loads as the DRCC-M model is generally more conservative. In Figure

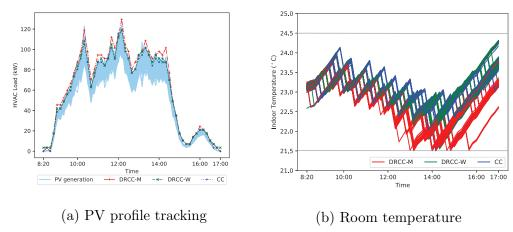


Figure 2 (Color online) PV profile tracking and room temperatures of 100 buildings under sunny weather

2b, we present the resulting room temperatures of all $N_{\text{HVAC}} = 100$ buildings over N_p periods for all three models. All the indoor temperatures are maintained within the desired comfort band [21.5, 24.5]°C. The DRCC models provide cooler room temperatures for most buildings which is an immediate result of turning on more HVAC units as shown in Figure 2a.

5.3. Out-of-Sample Performance

After solving all the models and obtaining the optimal schedules, we fix them in ten out-of-sample data sets, each consisting of N' = 1000 samples. For each data set, an out-of-sample probability is calculated as the ratio of the number of scenarios, where the PV generation is consumed locally (i.e., the total HVAC load is more than the PV generation), to the total number of scenarios N'. The performance is measured by the 95th percentile of probabilities of the ten out-of-sample sets.

To study the impact of the number of the samples used for solving the models, we consider two choices of the risk parameter $1-\alpha_t$: 80% and 50% under the sunny weather condition. We solve the three models using 10 samples and 100 samples, respectively, with the two risk levels. The out-of-sample performance is presented in Figure 3. When the sample size is small N=10, except for the DRCC-M model, both the DRCC-W and CC models fail to achieve the required risk level. For example, in Figure 3a, the DRCC-W and the CC models perform below the required risk level $1-\alpha_t=50\%$ between 11 am and 12 pm when using only 10 samples. However, with more samples N=100, the DRCC-W model is always above $1-\alpha_t=50\%$, while, the CC model sometimes still

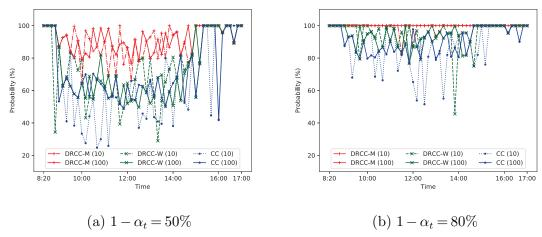


Figure 3 (Color online) Probability of locally consuming PV generation under sunny weather

fails to achieve the required risk level. Overall, the DRCC models perform better than the CC model, which is consistent with the previous observations. The DRCC-W models are more sensitive to the number of samples compared to the DRCC-M model. A comparison of sunny and cloudy weather is included in the online appendix K.

6. Studies on the Adjustable DRCC Models

In this section, we focus on the adjustable variants of the two DRCC models, where we consider the risk parameter α_t as a variable than a known parameter. Specifically, we solve the DRCC-W models using the two MILP formulations proposed in Section 3.2. The computational details of the adjustable models under the Wassestein set and the moment-based set are in the online appendices H and I. In Section H, the comparison of CPU time and optimality gaps can be found.

We now study the impact of the coefficient cost c_t in the objective (19a) of risk level α_t for both DRCC-M and DRCC-W models. We vary the coefficient from 10 to 20 in increments of 2. For the adjustable models, we observe that the optimal risk levels for the periods between 9:30 am and 2:30 pm are relatively lower. That is, during these periods, it is harder to consume all PV generation, which is consistent with the observations in Section 5.3 for the non-adjustable models. Therefore, we focus on these periods in between 9:30 am and 2:30 pm of a day with an increment of one hour.

In Figure 4, we show the risk levels under different choices of coefficient c_t for the DRCC-M and DRCC-W models. In Figures 4a and 4b, the value c_t of the risk level increases as larger coefficient is

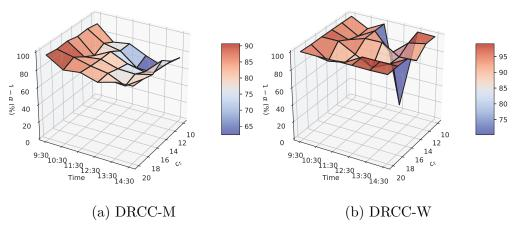


Figure 4 (Color online) The impact of the coefficient cost c_t on the risk level

set. The graph in Figure 4a of the DRCC-M model is flatter as c_t changes, because the performance of the DRCC-M model is less sensitive to the choice of c_t . While, as shown in Figure 4b, the DRCC-W model has a low risk level when c_t is small and a higher risk level when c_t is large.

In Figure 5, we show the objective costs for the various coefficient costs c_t . We see that both models yield higher objective costs as c_t increases. We also see that the DRCC-M model yields higher objective costs under large c_t even when the risk level is set lower than the DRCC-W model. For example, at 2:30 pm under $c_t = 20$, DRCC-M sets the risk level around 85% with an objective cost around 120, while DRCC-W achieves a higher risk level above 95% with an objective cost less than 90. This is expected as the DRCC-M model is more conservative and requires more HVAC units to run to achieve a similar risk level.

7. Conclusions

In this paper, we formulated a single-period BLC problem as a DRCC problem with uncertain PV generation under both the moment-based and Wasserstein ambiguity sets as DRCC-M and DRCC-W, respectively. For the moment-based ambiguity set, we reformulated the DRCC problem as an MILP reformulation. For the Wasserstein ambiguity set, we provided an MILP1 reformulation and a more compact MILP2 reformulation by exploiting the CVaR interpretation. The results for DRCC apply to general individual DR chance constraints with RHS uncertainty.

By considering the risk level as a decision variable, we also proposed adjustable DRCC formulations that determine the optimal risk level of the chance constraint to balance the total cost

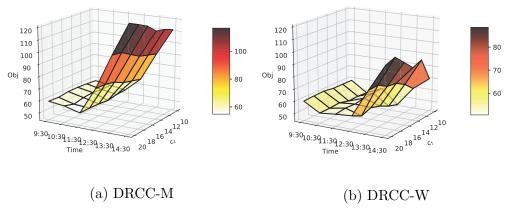


Figure 5 (Color online) The impact of the coefficient cost c_t on the objective cost

and overall performance. For the moment-based ambiguity set, we developed an exact solution approach by solving two SOCP problems. For the Wasserstein ambiguity set, we derived a big-M MILP reformulation and a big-M-free MILP reformulation. The results of the adjustable variants also apply to general individual binary chance constraints with RHS uncertainty.

Extensive computational studies were conducted on the non-adjustable and adjustable DRCC models under the two ambiguity sets. We found that the DRCC models achieve better out-sample performance while maintaining the indoor temperature within a desired comfort band. Specifically, the DRCC-M model requires fewer samples to achieve the required risk level. The DRCC-W model performs well when using enough many samples and only requires modest CPU time when solving the more compact reformulation MILP2. Furthermore, for the adjustable DRCC problem, we find that the DRCC-M is less sensitive to the choice of c_t while it may require higher objective costs.

References

Alhaider M, Fan L, Miao Z (2016) Benders decomposition for stochastic programming-based PV/battery/HVAC planning. 2016 IEEE Power and Energy Society General Meeting (PESGM), 1–5 (IEEE).

Barooah P (2019) Virtual energy storage from flexible loads: Distributed control with QoS constraints. *Smart Grid Control*, 99–115 (Springer).

Belić F, Hocenski Ž, Slišković D (2016) Thermal modeling of buildings with RC method and parameter estimation. 2016 International Conference on Smart Systems and Technologies (SST), 19–25 (IEEE).

- Chen Z, Kuhn D, Wiesemann W (2018) Data-driven chance constrained programs over Wasserstein balls.

 ArXiv arXiv:1809.00210, URL http://arxiv.org/abs/1809.00210.
- Chen Z, Wu L, Fu Y (2012) Real-time price-based demand response management for residential appliances via stochastic optimization and robust optimization. *IEEE Transactions on Smart Grid* 3(4):1822–1831.
- Conti J, Holtberg P, Diefenderfer J, LaRose A, Turnure JT, Westfall L (2016) International energy outlook 2016 with projections to 2040. Technical report, Washington, DC: Energy Information Administration (EIA), US Department of Energy.
- Cui B, Fan C, Munk J, Mao N, Xiao F, Dong J, Kuruganti T (2019) A hybrid building thermal modeling approach for predicting temperatures in typical, detached, two-story houses. Applied energy 236:101– 116.
- Delage E, Ye Y (2010) Distributionally robust optimization under moment uncertainty with application to data-driven problems. *Operations Research* 58(3):595–612.
- Diekerhof M, Peterssen F, Monti A (2017) Hierarchical distributed robust optimization for demand response services. *IEEE Transactions on Smart Grid* 9(6):6018–6029.
- Dong J, Olama M, Kuruganti T, Nutaro J, Winstead C, Xue Y, Melin A (2018) Model predictive control of building on/off HVAC systems to compensate fluctuations in solar power generation. 2018 9th IEEE International Symposium on Power Electronics for Distributed Generation Systems (PEDG), 1–5 (IEEE).
- Dong J, Olama MM, Kuruganti T, Nutaro J, Xue Y, Sharma I, Djouadi SM (2017) Adaptive building load control to enable high penetration of solar photovoltaic generation. *Power & Energy Society General Meeting*, 2017 IEEE, 1–5 (IEEE).
- Duan C, Fang W, Jiang L, Yao L, Liu J (2018) Distributionally robust chance-constrained approximate AC-OPF with Wasserstein metric. *IEEE Transactions on Power Systems* 33(5):4924–4936.
- Elçi Ö, Noyan N, Bülbül K (2018) Chance-constrained stochastic programming under variable reliability levels with an application to humanitarian relief network design. *Computers & Operations Research* 96:91–107.

- Esfahani PM, Kuhn D (2018) Data-driven distributionally robust optimization using the Wasserstein metric:

 Performance guarantees and tractable reformulations. *Mathematical Programming* 171(1-2):115–166.
- Evers WH (1967) A new model for stochastic linear programming. Management Science 13(9):680-693.
- Gaunt C, Namanya E, Herman R (2017) Voltage modelling of LV feeders with dispersed generation: Limits of penetration of randomly connected photovoltaic generation. *Electric Power Systems Research* 143:1–6.
- Guo Y, Wang S, Taha A, Summers T (2020) Optimal pump control for water distribution networks via data-based distributional robustness. ArXiv preprint arXiv:2005.08382, URL http://arxiv.org/abs/2003.12685.
- Hao H, Sanandaji BM, Poolla K, Vincent TL (2014) Aggregate flexibility of thermostatically controlled loads. IEEE Transactions on Power Systems 30(1):189–198.
- Hao H, Wu D, Lian J, Yang T (2017) Optimal coordination of building loads and energy storage for power grid and end user services. *IEEE Transactions on Smart Grid* 9(5):4335–4345.
- Ho-Nguyen N, Kılınç-Karzan F, Küçükyavuz S, Lee D (2021) Distributionally robust chance-constrained programs with right-hand side uncertainty under Wasserstein ambiguity. *Mathematical Programming* 1–32.
- Hughes JT, Domínguez-García AD, Poolla K (2015) Virtual battery models for load flexibility from commercial buildings. 2015 48th Hawaii International Conference on System Sciences, 2627–2635 (IEEE).
- Kocaman AS, Ozyoruk E, Taneja S, Modi V (2020) A stochastic framework to evaluate the impact of agricultural load flexibility on the sizing of renewable energy systems. *Renewable Energy* 152:1067–1078.
- Lejeune MA, Shen S (2016) Multi-objective probabilistically constrained programs with variable risk: Models for multi-portfolio financial optimization. *European Journal of Operational Research* 252(2):522–539.
- Lu N (2012) An evaluation of the HVAC load potential for providing load balancing service. *IEEE Transactions on Smart Grid* 3(3):1263–1270.
- Lu S, Gu W, Meng K, Dong Z (2020) Economic dispatch of integrated energy systems with robust thermal comfort management. *IEEE Transactions on Sustainable Energy* 12(1):222–233.
- Luedtke J, Ahmed S (2008) A sample approximation approach for optimization with probabilistic constraints.

 SIAM Journal on Optimization 19(2):674–699.

- Ma H, Jiang R, Yan Z (2019) Distributionally robust co-optimization of power dispatch and do-not-exceed limits. *IEEE Transactions on Power Systems* 35(2):887–897.
- Mark C, Liu S (2020) Stochastic MPC with distributionally robust chance constraints. *IFAC-PapersOnLine* 53(2):7136–7141.
- Mathieu JL, Koch S, Callaway DS (2013) State estimation and control of electric loads to manage real-time energy imbalance. *IEEE Transactions on Power Systems* 28(1):430–440.
- Nguyen DT, Le LB (2014) Risk-constrained profit maximization for microgrid aggregators with demand response. *IEEE Transactions on smart grid* 6(1):135–146.
- Nguyen DT, Nguyen HT, Le LB (2014) Coordinated dispatch of renewable energy sources and HVAC load using stochastic programming. Smart Grid Communications (SmartGridComm), 2014 IEEE International Conference on, 139–144 (IEEE).
- Qiu F, Li Z, Wang J (2016) A data-driven approach to improve wind dispatchability. *IEEE Transactions on Power Systems* 32(1):421–429.
- Ruszczyński A (2002) Probabilistic programming with discrete distributions and precedence constrained knapsack polyhedra. *Mathematical Programming* 93(2):195–215.
- Shen S (2014) Using integer programming for balancing return and risk in problems with individual chance constraints. *Computers & operations research* 49:59–70.
- Smith JE, Winkler RL (2006) The optimizer's curse: Skepticism and postdecision surprise in decision analysis.

 *Management Science 52(3):311–322.
- Stinner S, Huchtemann K, Müller D (2016) Quantifying the operational flexibility of building energy systems with thermal energy storages. *Applied Energy* 181:140–154.
- Teodorescu R, Liserre M, Rodriguez P (2011) Grid converters for photovoltaic and wind power systems, volume 29 (John Wiley & Sons).
- Wang J, Huang S, Wu D, Lu N (2020) Operating a commercial building HVAC load as a virtual battery through airflow control. *IEEE Transactions on Sustainable Energy* 12(1):158–168.
- Wang Z, Shen C, Liu F, Wang J, Wu X (2018) An adjustable chance-constrained approach for flexible ramping capacity allocation. *IEEE Transactions on Sustainable Energy* 9(4):1798–1811.

- Wijayasekara D, Manic M (2015) Data-fusion for increasing temporal resolution of building energy management system data. IECON 2015-41st Annual Conference of the IEEE Industrial Electronics Society, 004550–004555 (IEEE).
- Xie W (2019) On distributionally robust chance constrained programs with Wasserstein distance. *Mathemati-* cal Programming 1–41, URL http://dx.doi.org/https://doi.org/10.1007/s10107-019-01445-5.
- Xie Jiang (2019)Optimized Bonferroni Ahmed S. \mathbf{R} approximations of distributionally robust joint chance constraints. MathematicalProgramming 1-34, URL http://dx.doi.org/https://doi.org/10.1007/s10107-019-01442-8.
- Yang I (2019) Data-driven distributionally robust stochastic control of energy storage for wind power ramp management using the Wasserstein metric. *Energies* 12(23):4577.
- Yin R, Kara EC, Li Y, DeForest N, Wang K, Yong T, Stadler M (2016) Quantifying flexibility of commercial and residential loads for demand response using setpoint changes. *Applied Energy* 177:149–164.
- Žáčeková E, Váňa Z, Cigler J (2014) Towards the real-life implementation of MPC for an office building: Identification issues. *Applied Energy* 135:53–62.
- Zhang H, Hu Z, Munsing E, Moura SJ, Song Y (2018a) Data-driven chance-constrained regulation capacity offering for distributed energy resources. *IEEE Transactions on Smart Grid* 10(3):2713–2725.
- Zhang Y, Dong J, Kuruganti T, Shen S, Xue Y (2019) Distributionally robust building load control to compensate fluctuations in solar power generation. 2019 American Control Conference (ACC), 5857–5863 (IEEE).
- Zhang Y, Jiang R, Shen S (2018b) Ambiguous chance-constrained binary programs under mean-covariance information. SIAM Journal on Optimization 28(4):2922–2944.
- Zhang Y, Shen S, Mathieu JL (2016) Distributionally robust chance-constrained optimal power flow with uncertain renewables and uncertain reserves provided by loads. *IEEE Transactions on Power Systems* 32(2):1378–1388.
- Zhao C, Jiang R (2018) Distributionally robust contingency-constrained unit commitment. *IEEE Transactions on Power Systems* 33(1):94–102.

Appendices

A. Proof of Theorem 2

Proof of Theorem 2: We first rearrange constraint (20) as

$$\sum_{\ell=1}^{N_s} P_{\ell} u_{t,\ell} - \theta_t - \sigma_t \sqrt{\gamma_1} \ge \left(\sqrt{\frac{1 - \alpha_t}{\alpha_t} (\gamma_2 - \gamma_1)}\right) \sigma_t. \tag{30}$$

Given the nonnegative RHS of (30), the left-hand side is implicitly enforced nonnegative, which results in constraint (21c). By squaring both side, we obtain

$$(\gamma_2 - \gamma_1)\sigma_t^2 \le \alpha_t \left[\left(\sum_{\ell=1}^{N_{\text{HVAC}}} P_\ell u_{t,\ell} - \theta_t - \sigma_t \sqrt{\gamma_1} \right)^2 + (\gamma_2 - \gamma_1)\sigma_t^2 \right]. \tag{31}$$

The RHS of (31) is nonlinear. We let $d = \left(\sum_{\ell=1}^{N_{\text{HVAC}}} P_{\ell} u_{t,\ell} - \theta_t - \sigma_t \sqrt{\gamma_1}\right)^2 + (\gamma_2 - \gamma_1)\sigma_t^2$. Then inequality (31) is equivalent to $(\gamma_2 - \gamma_1)\sigma_t^2 \leq \alpha_t d$ which is equivalent to (21a). To linearize d, we define $g_{ij} := u_{t,i} u_{t,j}$ by McCormick inequalities (21d). We conclude the proof. \square

B. Proof of Theorem 3

Proof of Theorem 3: To show the equivalence, we need to show that (i) constraint (22) implies constraints (23a)–(23d) and (ii) constraints (23a)–(23d) imply constraint (22).

(i)
$$(22) \rightarrow (23a)-(23d)$$
.

Given a solution (u_t^*, α_t^*) that satisfies (22), we let $\phi^* = \sqrt{1/\alpha_t^*}$, $w^* = \sqrt{\phi^*}$, $q^* = 1/w^*$. Then $(u_t^*, \alpha_t^*, \phi^*, w^*, q^*)$ is a solution to (23a)–(23d).

(ii) $(23a)-(23d) \rightarrow (22)$.

We notice that (23b) is equivalent to

$$\alpha_t \phi \ge q^2, \ \phi \ge 0; \tag{32}$$

and (23d) can be rewritten as

$$q \ge \frac{1}{w}, \ w \ge 0. \tag{33}$$

Combining (32), (33), and (23c), we have $\alpha_t \phi \geq 1/\phi$, which is further equivalent to

$$v \ge \sqrt{\frac{1}{\alpha_t}}. (34)$$

Combining (23a) and (34), we conclude that constraint (23a) implies (22). \Box

C. Proof of Theorem 4

Proof of Theorem 4: In the adjustable DRCC model (19), we replace the adjustable DR chance constraint (19b) with the following convex reformulation.

$$\sum_{\ell=1}^{N_{\text{HVAC}}} P_{\ell} u_{t,\ell} - \theta_t - \sigma_t \sqrt{\gamma_1} \ge \sigma_t \sqrt{\gamma_2 - \gamma_1} r \tag{35}$$

$$r \ge \sqrt{\frac{1 - \alpha_t}{\alpha_t}}. (36)$$

The RHS of constraint (36) is convex when $0 \le \gamma_1/\gamma_2 \le \alpha_t \le 0.75$ as the second-order derivative $(3-4\alpha_t)(1-\alpha_t)^{-3/2}\alpha_t^{-5/2}/4$ is non-negative. We can further construct an outer approximation of the reformulation (35)–(36) by replacing (36) with

$$2r \ge \sqrt{\frac{1}{\alpha_t}}. (37)$$

Constraint (37) is implied by (36) when $\alpha_t \leq 0.75$. Using a similar proof of Theorem 3, we can show that (37) is equivalent to constraints (24b) – (24e).

D. Proof of Proposition 3

Proof of Proposition 3: To show that $Z = Z_1$, we need to show that $Z \subseteq Z_1$ and $Z_1 \subseteq Z$.

(i) $Z \subseteq Z_1$.

Given $u_t \in \mathbb{Z}$, there exists $\gamma \geq 0$ such that (u_t, γ) satisfies (9a) and (9b). If $\gamma > 0$, let $\lambda = 1/\gamma$. It is easy to see that (u_t, λ) satisfies (25a) and (25b). For the case $\gamma = 0$, (9a) is equivalent to

$$\left\{ u_t: \ \delta_t \leq \frac{1}{N} \sum_{n=1}^N \min \left\{ 0, \ \max \left[\sum_{\ell=1}^{N_{\text{HVAC}}} P_\ell u_{t,\ell} - P_{total,t}^n, 0 \right] \right\} \right\} = \left\{ u_t: \ \delta_t \leq 0 \right\}.$$

Since $\delta_t > 0$, the left-hand side of (D) is equivalent to an empty set.

(ii) $Z_1 \subseteq Z$.

Given $u_t \in Z_1$, there exists $\lambda \ge 0$ such that (u_t, λ) satisfies (25a) and (25b). Similarly, if $\lambda > 0$, we let $\gamma = 1/\lambda$, which satisfies (9a) and (9b). In the case $\lambda = 0$, (25) is equivalent to

$$\{u_t: \alpha_t \geq 1\}$$

which is empty. \Box

E. Proof of Theorem 5

Proof: According to Theorem 1 and Proposition 2, for a given pair of u_t and α_t which is feasible for the adjustable DR chance constraint (19b), there exists a (j, k) pair such that

$$k/N \le \alpha_t < (k+1)/N \tag{38}$$

$$P_{\text{total},t}^{(j)} < \sum_{\ell=1}^{N_{\text{HVAC}}} P_{\ell} u_{t,\ell} \le P_{\text{total},t}^{(j-1)} \tag{39}$$

$$-\frac{1}{N} \sum_{n=j}^{k} \left(P_{\text{total},t}^{(k+1)} - P_{\text{total},t}^{(n)} \right) - \left(\alpha_t - \frac{j-1}{N} \right) \left(\sum_{\ell=1}^{N_{\text{HVAC}}} P_\ell u_{t,\ell} - P_{\text{total},t}^{(k+1)} \right) \le -\delta. \tag{40}$$

We denote $\Delta_{jk} \in \{0,1\}$ for all $0 \le j-1 \le k \le N-1$ such that $\Delta_{jk} = 1$ if we select j and k as the critical index pair; $\Delta_{jk} = 0$, otherwise. To impose constraint (40), we require

$$\sum_{j=1}^{N} \sum_{k=j-1}^{N-1} \left[-\frac{1}{N} \sum_{n=j}^{k} \left(P_{\text{total},t}^{(k+1)} - P_{\text{total},t}^{(n)} \right) - \left(\alpha_t - \frac{j-1}{N} \right) \left(\sum_{\ell=1}^{N_{\text{HVAC}}} P_\ell u_{t,\ell} - P_{\text{total},t}^{(k+1)} \right) \right] \Delta_{jk} \le -\delta. \tag{41}$$

Constraint (41) is nonlinear due to two bilinear terms, i.e., $\alpha_t \Delta_{jk}$ and $u_{t,\ell} \Delta_{jk}$, and one trilinear term, $\alpha_t u_{t,\ell} \Delta_{jk}$. To linearize them, we introduce $\varepsilon_{jk} = \alpha_t \Delta_{jk}$, $\tau_{\ell jk} = u_{t,\ell} \Delta_{ji}$, $o_{\ell jk} = \alpha_t u_{t,\ell} \Delta_{jk}$ for $0 \le j-1 \le k \le N-1, 1 \le \ell \le N_{\text{HVAC}}$, and the McCormick inequalities (29e)–(29g).

To ensure the feasibility of the solution (u_t, α_t) associated with a (j, k) pair (there can be multiple solutions associated with one (j, k) pair), we need to further satisfy (38) and (39), which is equivalent to (29c) and (29d). Therefore, we conclude the proof.

F. DRCC Model with the Decision of Fleet Size

In this section, we present a DRCC model that incorporates the decision of the fleet size of residential HVAC units, N_{HVAC} , which is a given parameter in previous models. We associate N_{HVAC} with a unit penalty cost $c_{N_{\text{HVAC}}}$ in the objective coefficients. We denote $N_{\text{HVAC}}^{\text{U}}$ the maximum number of the HVAC units we can deploy to consume the PV generation. For HVAC unit $j, j = 1, ..., N_{\text{HVAC}}^{\text{U}}$, we introduce a logical binary variable ζ_j such that $\zeta_j = 1$, if unit j belongs to the fleet, and 0 otherwise. The DRCC model is formulated as follows.

$$\min_{N_{\text{HVAC}}, u_t, \beta_{t,\ell}, x_{t,\ell} t = 1, \dots, N_p} \sum_{t=1}^{N_p} \left[c_{\text{sys}} \sum_{\ell=1}^{N_{\text{HVAC}}^{\text{U}}} \beta_{t,\ell} + c_{\text{switch}} \sum_{\ell=1}^{N_{\text{HVAC}}^{\text{U}}} u_{t,\ell} \right] + c_{N_{\text{HVAC}}} N_{\text{HVAC}}$$
(42a)

s.t.
$$(3c) - (3e)$$
 for $t = 1, ..., N_p$

$$\inf_{f \in \mathcal{D}_t} \mathbb{P}\left(\sum_{\ell=1}^{N_{\text{HVAC}}^{\text{U}}} P_\ell u_{t,\ell} - \sum_{i=1}^{N_{\text{PV}}} \widetilde{P}_{\text{PV},t,i} \ge 0\right) \ge 1 - \alpha_t \text{ for } t = 1, ..., N_p \text{ (42b)}$$

$$\zeta_{\ell} \le \sum_{t=1}^{N_p} u_{t,\ell} \le N_p \zeta_{\ell}, \ \ell = 1, \dots, N_{\text{HVAC}}^{\text{U}}$$
(42c)

$$\sum_{\ell=1}^{N_{\rm HVAC}^{\rm U}} \zeta_{\ell} \le N_{\rm HVAC} \tag{42d}$$

$$x_{1,\ell} = A_{\ell} x_{0,\ell} \zeta_{\ell} + B_{\ell} u_{1,\ell} + G_{\ell} v_{\ell} \zeta_{\ell} + (1 - \zeta_{\ell}) x_{\text{ref}}, \ \ell = 1, \dots, N_{\text{HVAC}}^{\text{U}}$$
 (42e)

$$x_{t,\ell} = A_{\ell}(x_{t-1,\ell} - x_{\text{ref}} + x_{\text{ref}}\zeta_{\ell}) + B_{\ell}u_{t,\ell} + G_{\ell}v_{\ell}\zeta_{\ell} + (1 - \zeta_{j})x_{\text{ref}},$$

$$t = 2, \dots, N_p, \ \ell = 1, \dots, N_{\text{HVAC}}^{\text{U}}$$
 (42f)

$$0 \le N_{\text{HVAC}} \le N_{\text{HVAC}}^{\text{U}} \tag{42g}$$

$$\zeta \in \{0, 1\}^{N_{\text{HVAC}}^{\text{U}}}.\tag{42h}$$

Constraint (42c) requires all $u_{t,\ell}$ s' being zeros if $\zeta_{\ell} = 0$ and thus the HVAC unit ℓ is not in the fleet. Constraints (42e) and (42f) ensure that for HVAC unit ℓ not in the fleet, i.e., $\zeta_{\ell} = 0$, the indoor temperatures $x_{t,\ell}$ over all N_p periods are imposed to be x_{ref} and thus contribute zero to the objective value. We remark that (42) is a multi-period model over all N_p periods with individual DR chance constraints to guarantee the utilization of the PV generation for each period. All the solution methods and modeling techniques in Sections 2 and 3 can still be applied to (42).

G. CPU Time and Optimality Gaps for Wasserstein Set \mathcal{D}_t^2 : Low Risk Requirement $1-\alpha_t$

See Table 3.

H. CPU Time and Optimality Gaps for Adjustable DRCC under Wasserstein Set \mathcal{D}_t^2

Following the in-sample data generation procedure in Section 4, we generate 10 instances (each of 10 samples) under the sunny weather condition and solve them using DRCC-W models by MILP3 and MILP4 reformulations, respectively. The CPU time limit for each period is 100 seconds. In Table 4, MILP4 solves all instances faster with an average of 1154.29 seconds than 3449.39 seconds

Table 3 Comparison of CPU time (in seconds) and optimality gaps of low risk requirement $1-\alpha_t$

					`	,		,		· · · · · · · · · · · · · · · · · · ·
$1 - \alpha$	δ			N = 100			N = 500		N = 3	3000
		Instance	MILP1	MILP-H	MILP2	MILP1	MILP-H	MILP2	MILP-H	MILP2
		1	122.45 (1, 0.21%)	6.22	0.84	2517.31 (9, 13.48%)	165.35	3.88	2065.91 (14, 5.47%)	38.27
		2	122.61 (1, 0.34%)	12.49	0.81	2177.88 (6, 6.02%)	226.12	4.48	2116.55 (16, 3.36%)	47.35
		3	125.81 (1, 0.29%)	14.49	0.87	2328.41 (5, 5.90%)	165.42	4.69	2382.27 (20, 4.25%)	45.83
		4	35.72	10.88	0.74	2186.71 (3, 0.43%)	179.87	3.95	$2447.35\ (20, 6.34\%)$	46.88
		5	65.05	4.02	0.86	2369.65 (6, 23.48%)	202.62	4.17	1973.34 (16, 4.01%)	42.08
10%	0.02	6	24.46	8.07	0.80	2780.93 (15, 19.66%)	205.48	4.51	2347.32 (19, 4.27%)	$142.53\ (1,\ 0.38\%)$
		7	123.33 (1, 0.46%)	11.19	0.89	2528.08 (9, 8.65%)	$247.28\ (1,\ 0.44\%)$	4.30	2417.75 (21, 4.41%)	46.65
		8	27.46	5.32	0.89	2339.40 (6, 9.09%)	$211.23\ (1, 0.43\%)$	4.73	2126.13 (17, 4.83%)	42.37
		9	123.79 (1, 0.40%)	8.55	0.82	2201.85 (5, 12.77%)	202.42	5.02	2128.63 (17, 3.04%)	39.75
		10	32.43	4.76	0.87	2361.87 (5, 4.60%)	152.37	4.44	2049.74 (16, 5.46%)	44.98
		Avg.	80.31 (0.5, 0.17%)	8.60	0.84	2379.21 (6.9, 10.41%)	195.82 (0.2, 0.09%)	4.42	2205.50 (17.6, 4.54%)	53.67 (0.1, 0.04%)
		1	373.90 (2, 0.47%)	138.07 (1, 0.32%)	1.49	3113.95 (11, 14.50%)	489.31 (2, 0.39%)	9.77	3148.18 (25, 6.60%)	219.03 (1, 0.32%)
		2	312.83 (2, 0.27%)	120.61 (1, 0.30%)	4.02	3182.16 (12, 27.09%)	314.02 (2, 0.39%)	10.51	2694.06 (19, 5.38%)	295.30 (2, 0.26%)
		3	346.11 (2, 0.50%)	209.01 (1, 0.32%)	5.26	3146.71 (12, 19.78%)	328.88 (2, 0.39%)	10.07	2854.40 (23, 5.97%)	232.00 (1, 0.30%)
		4	316.45 (2, 0.39%)	221.34 (2, 0.38%)	8.86	3171.33 (8, 22.25%)	315.03 (2, 0.39%)	9.52	2388.50 (17, 4.98%)	221.34 (1, 0.29%)
		5	317.72 (2, 0.41%)	180.47 (1, 0.31%)	7.84	3119.98 (12, 26.54%)	412.70 (2, 0.39%)	9.97	2847.15 (20, 4.53%)	215.50 (1, 0.28%)
10%	0.2	6	246.86 (1, 0.43%)	110.10 (1, 0.42%)	1.55	3447.02 (15, 20.60%)	450.19 (2, 0.39%)	10.15	2885.27 (26, 5.42%)	298.43 (2, 0.22%)
		7	319.89 (2, 0.36%)	215.01 (2, 0.36%)	3.06	3215.30 (10, 16.71%)	442.92 (2, 0.38%)	9.92	2594.05 (20, 6.33%)	246.34 (1, 0.04%)
		8	224.64 (1, 0.33%)	256.21 (2, 0.38%)	1.59	3172.53 (14, 12.03%)	367.06 (2, 0.39%)	9.59	2781.21 (18, 6.75%)	303.22 (2, 0.38%)
		9	300.75 (2, 0.29%)	209.17 (2, 0.34%)	4.61	3134.99 (13, 28.85%)	396.29 (2, 0.39%)	10.15	3099.77 (26, 5.98%)	214.39 (1, 0.28%)
		10	333.62 (2, 0.39%)	213.95 (2, 0.37%)	1.38	3293.18 (12, 14.70%)	361.87 (2, 0.39%)	10.44	2686.10 (21, 5.77%)	229.30 (1, 0.32%)
		Avg.	309.28 (1.8, 0.38%)	187.39 (1.5, 0.35%)	3.97	3199.71 (11.9, 20.31%)	387.83 (2, 0.39%)	10.01	2797.87 (21.5, 5.77%)	247.49 (1.3, 0.27%)
		1	34.97	5.71	0.87	3278.54 (19, 27.73%)	184.14	4.70	2125.15 (14, 4.82%)	43.55
		2	39.86	9.98	0.83	3010.49 (17, 24.43%)	143.21	4.38	2203.64 (16, 3.62%)	35.64
		3	135.69 (1, 0.29%)	8.97	0.99	3100.17 (15, 34.20%)	155.43	4.72	1984.68 (15, 3.85%)	35.80
		4	137.47 (1, 0.38%)	6.40	0.85	3061.05 (15, 28.30%)	131.96	4.23	2248.16 (17, 5.22%)	36.90
		5	138.02 (1, 0.17%)	17.55	0.77	2870.46 (16, 31.43%)	208.30	4.23	2131.41 (17, 3.90%)	35.71
20%	0.02	6	79.53	10.39	0.73	3068.02 (14, 24.83%)	177.49	5.52	1643.78 (11, 2.93%)	34.87
		7	64.93	8.82	0.80	2823.78 (9, 15.16%)	317.74 (1, 0.32%)	104.82 (1, 0.10%)	1981.36 (15, 5.53%)	29.77
		8	231.45 (2, 0.19%)	105.15 (1, 0.31%)	0.80	2850.97 (14, 35.39%)	236.45	5.70	1799.90 (10, 4.67%)	32.08
		9	134.99 (1, 0.36%)	108.33 (1, 0.31%)	1.15	3017.16 (11, 25.05%)	217.58 (1, 0.31%)	4.48	1996.12 (16, 5.39%)	33.86
		10	136.47 (1, 0.22%)	12.35	0.79	2715.52 (9, 13.52%)	89.89	4.19	2185.03 (18, 5.88%)	37.21
		Avg.	113.34 (0.7, 0.16%)	29.36 (0.2, 0.06%)	0.86	2979.62 (13.9, 26.00%)	186.22 (0.2, 0.06%)	14.70 (0.1, 0.01%)	2029.92 (14.9, 4.58%)	35.54
		1	388.77 (1, 0.31%)	43.8	1.47	3505.28 (11, 24.82%)	200.31 (1, 0.36%)	10.38	3277.78 (27, 3.97%)	196.14 (1, 0.29%)
		2	296.35 (1, 0.39%)	28.7	1.37	3547.98 (15, 18.34%)	268.09	40.14	3356.53 (28, 3.76%)	188.56 (1, 0.36%)
		3	309.24 (1, 0.34%)	37.9	1.40	3495.98 (16, 22.81%)	244.00	11.34	3468.97 (26, 3.80%)	290.79 (2, 0.28%)
		4	399.73 (2, 0.56%)	81.0	2.23	3354.51 (13, 27.32%)	226.25 (1, 0.36%)	15.48	3365.82 (27, 4.06%)	193.38 (1, 0.34%)
		5	286.19 (1, 0.37%)	11.4	1.51	3376.60 (13, 29.87%)	368.06 (1, 0.37%)	10.82	3527.95 (27, 4.97%)	183.83 (1, 0.27%)
20%	0.2	6	362.52 (1, 0.44%)	13.8	1.26	3384.83 (9, 33.56%)	298.02 (1, 0.36%)	110.27 (0.045%)	3354.24 (26, 4.17%)	189.52 (1, 0.27%)
2070	0.2	7	400.97 (1, 0.38%)	9.1	2.12	3474.31 (15, 23.25%)	337.58	83.60	3191.83 (27, 4.10%)	222.98 (1, 0.36%)
		8	424.35 (2, 0.42%)	9.9	1.56	3412.10 (11, 26.36%)	206.94 (1, 0.36%)	110.55 (1, 0.23%)	3447.36 (29, 4.11%)	187.14 (1, 0.23%)
		9	255.55	11.9	1.47	3412.99 (12, 26.23%)	283.64	28.68	3464.42 (29, 3.64%)	92.86
		10	326.42 (1, 0.34%)	11.0	1.38	3465.78 (14, 19.64%)	249.26 (1, 0.35%)	109.15 (1, 0.23%	3425.87 (27, 4.04%)	382.44 (3, 1.04%)
					1.58					
		Avg.	345.01 (1.1, 0.36%)	20.9	1.08	3443.04 (12.9, 25.22%)	200.21 (0.0, 0.22%)	55.04 (U.S, U.U0%)	3388.08 (27.3, 4.06%)	212.10 (1.2, U.34%)

of MILP3. Among the 53 periods solved, MILP3 has more periods not solved optimally. The average gap of the unsolved periods is up to 12.38%. While MILP4 only yields a gap of 0.73% as the MILP4 formulation provides a tighter linear relaxation than the MILP3.

Table 4 Comparison of CPU time (in seconds) and optimality gaps

		MILP3		MILP4				
Instance	CPU	# Limit	Gap	CPU	# Limit	Gap		
1	3410.35	33	12.35%	1165.00	8	0.70%		
2	3456.28	34	12.44%	1069.39	7	0.41%		
3	3460.71	33	12.84%	1557.45	13	0.68%		
4	3453.83	34	11.68%	1099.37	8	0.88%		
5	3486.60	34	12.13%	1307.64	11	0.77%		
6	3459.33	34	12.47%	1048.38	8	1.03%		
7	3461.45	34	12.43%	1380.35	11	0.76%		
8	3457.13	33	11.88%	1194.67	9	0.71%		
9	3392.60	33	12.57%	904.65	4	0.43%		
10	3455.67	33	13.00%	816.00	5	0.91%		
Avg.	3449.39	34	12.38%	1154.29	8	0.73%		

I. CPU Time and Optimality Gaps for Moment-based Ambiguity Set

In Table 5, the total CPU time of solving all 53 periods are reported for the DRCC and adjustable variants under the moment-based set \mathcal{D}_t^1 . We set $\gamma_1 = 0$, $\gamma_2 = 1$, and $1 - \alpha_t = 80\%$. Column "# Limit" indicates the number of periods that cannot be solved when the time limit is reached. The average optimality gaps of these (unsolved) periods are presented in the next column "Gap." For the adjustable DRCC, as $\gamma_1/\gamma_2 = 0$, only SOCP1 or SOCP3 is required. Note that in our problem settings, α_t does not exceed 75%. Therefore SOCP1 and SOCP3 are equivalent. For all instances,

Table 5 Comparison of CPU time (in seconds) and optimality gaps for DRCC and adjustable variants under \mathcal{D}_t^1

	DRCC			adjustable DRCC						
Instance					SOCP1		SOCP3			
	CPU	# Limit	Gap	CPU	# Limit	Gap	CPU	# Limit	Gap	
1	0.31	0	N/A	3566.69	31	5.19%	1243.26	12	0.06%	
2	0.26	0	N/A	3586.60	32	4.73%	1437.35	13	0.06%	
3	0.19	0	N/A	3525.74	29	5.22%	1554.54	14	0.09%	
4	0.32	0	N/A	3624.84	30	5.02%	1028.21	10	0.09%	
5	0.28	0	N/A	3536.61	30	5.17%	1455.35	13	0.07%	
6	0.27	0	N/A	3510.96	31	4.65%	1747.06	16	0.09%	
7	0.24	0	N/A	3589.61	31	4.79%	1352.62	13	0.09%	
8	0.32	0	N/A	3432.83	30	5.05%	925.62	9	0.08%	
9	0.28	0	N/A	3598.59	29	5.09%	1220.28	12	0.04%	
10	0.31	0	N/A	3607.45	32	5.10%	1107.61	10	0.11%	
Avg.	0.28	0	N/A	3557.99	31	5.00%	1307.19	12	0.08%	

SOCP3 yields shorter CPU times and smaller optimality gaps than SOCP1.

J. Tracking Performance and Room Temperatures for Cloudy Weather

Figure 6a shows the PV profile tracking under the cloudy weather. The three models track the PV profile well most of the time. Around 4:00 pm, when the PV generation is low, the optimal schedule of all three models do not track the PV generation as closely as before. In Figure 6b, again, all three models keep the room temperature within the comfort band and DRCC-M provides relatively lower temperature.

K. Out-of-sample Performance: Sunny vs. Cloudy

In Figure 7, the 95th percentile of probabilities are shown for all three models under the sunny and cloudy weather conditions. In both plots, the two DRCC models perform better than the CC models. Again, as the DRCC-M model is more conservative, the DRCC-M model achieves higher probability than the DRCC-W model.

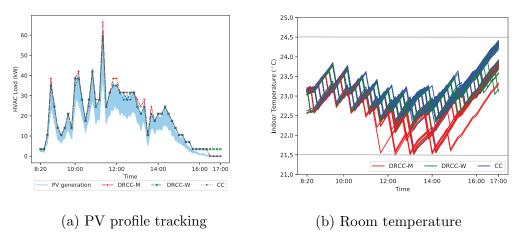


Figure 6 (Color online) PV profile tracking and room temperatures of 35 buildings under sunny weather

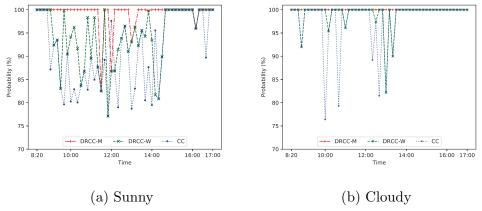


Figure 7 (Color online) Probabilities of locally consuming PV generation under sunny and cloudy weather conditions